Impact of the *fac*/*mer* isomerism on the excited-state dynamics of pyridyl-carbene Fe(II) complexes

Kevin Magra,[a] Edoardo Domenichini,[b] Antonio Francés-Monerris,[c] Cristina Cebrian,[a] Marc Beley,[d] Mohamed Darari,[d] Mariachiara Pastore,[c] Antonio Monari,[c] Xavier Assfeld,[c] Stefan Haacke[b] and Philippe C. Gros[,d]*

a) Université de Lorraine, CNRS, L2CM, F-57000 Metz, France. b) Université de Strasbourg, CNRS, IPCMS, F-67000 Strasbourg, France. c) Université de Lorraine, CNRS, LPCT, F-54000 Nancy, France, d) Université de Lorraine, CNRS, L2CM, F-54000 Nancy, France

Corresponding Author

*Philippe C. Gros: philippe.gros@univ-lorraine.fr

Supporting Information

Table of Contents

Characterization of products

General Considerations

Solvents and commercially available reagents were used as received. Thin layer chromatography (TLC) was performed by using silica gel 60 F-254 (Merck) plates and visualized under UV light. Chromatographic purification was performed by using silica gel 60 (0.063–0.2 mm/70–230 mesh). ^{1}H (400 MHz) and ^{13}C NMR (100 MHz) spectra were taken on a DRX400 Bruker spectrometer at ambient temperature. The chemical shifts (δ), were calibrated by using either tetramethylsilane (TMS) or signals from the residual protons of the deuterated solvents and are reported in parts per million (ppm) from low to high field. High-resolution mass spectrometry (HRMS) data was obtained by using Bruker micrOTOF-Q spectrometer. UV-vis spectra were recorded in a 1 cm path length quartz cell on a LAMBDA 1050 (Perkin Elmer), spectrophotometer. Cyclic voltammetry was performed on a Radiometer PST006 potentiostat using a conventional three-electrode cell. The saturated calomel electrode (SCE) was separated from the test compartment using a bridge tube. The solutions of studied complexes (0.2 mM) were purged with argon before each measurement. The test solution was acetonitrile containing 0.1 M Bu_4NPF_6 as supporting electrolyte. The working electrode was a vitreous carbon rod ($1cm^2$) wire and the counter-electrode was a 1 cm^2 Pt disc. After the measurement, ferrocene was added as the internal reference for calibration. All potentials were quoted versus SCE. In these conditions the redox potential of the couple Fc+/Fc was found at 0.39V. In all the experiments the scan rate was 100mV/s.

N-(Et-Im-Py)$_3$(PF$_6$)$_3$ **, L2**

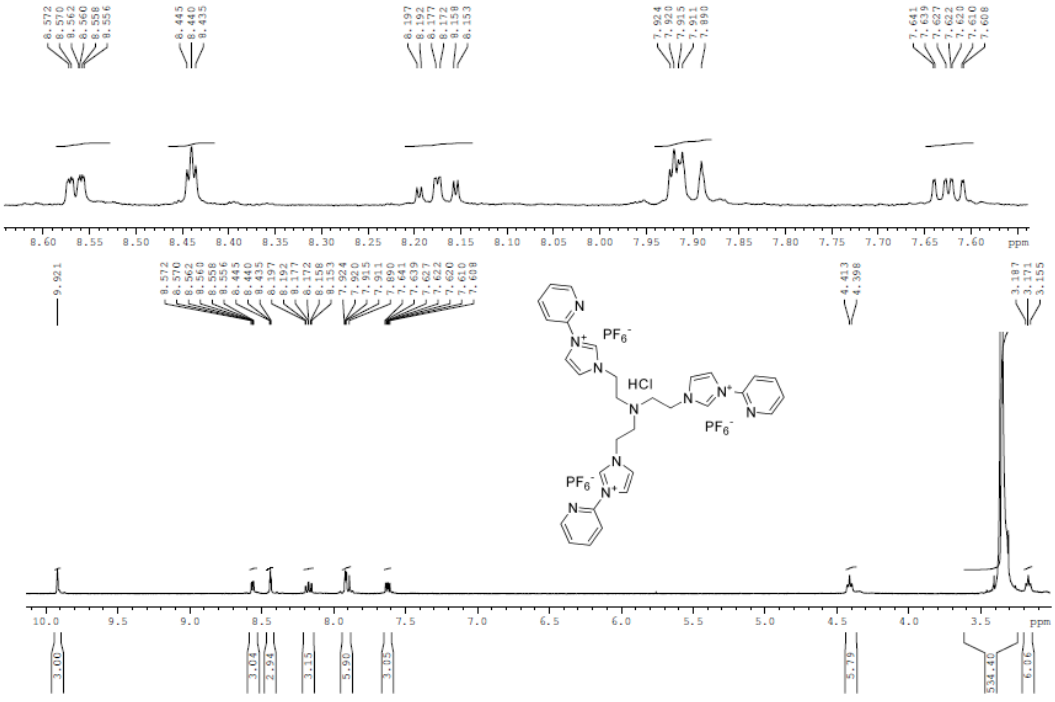

Figure S1. ^{1}H-NMR spectrum of the ligand N-(Et-Im-Py)$_3$(PF$_6$)$_3$ in DMSO-d$_6$.

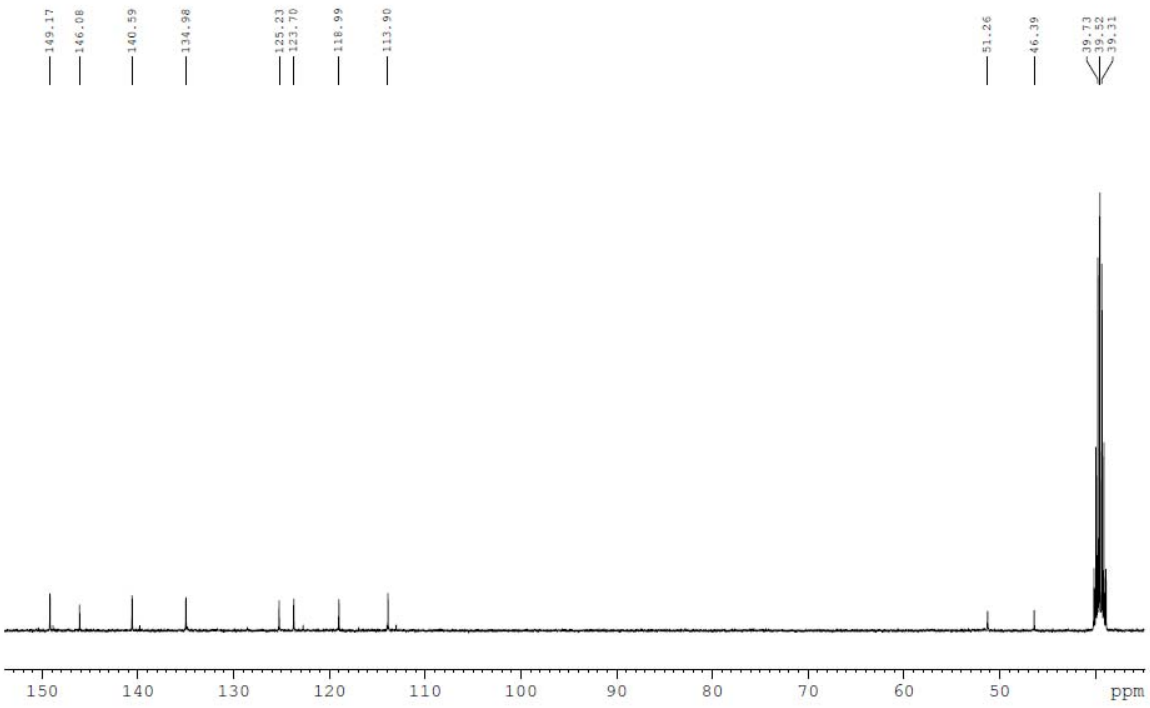

Figure S2. ^{13}C-NMR spectrum of the ligand N-(Et-Im-Py)$_3$(PF$_6$)$_3$ in DMSO-d$_6$.

[Fe(Me-Im-Py)$_3$](PF$_6$)$_2$, **C1 :**

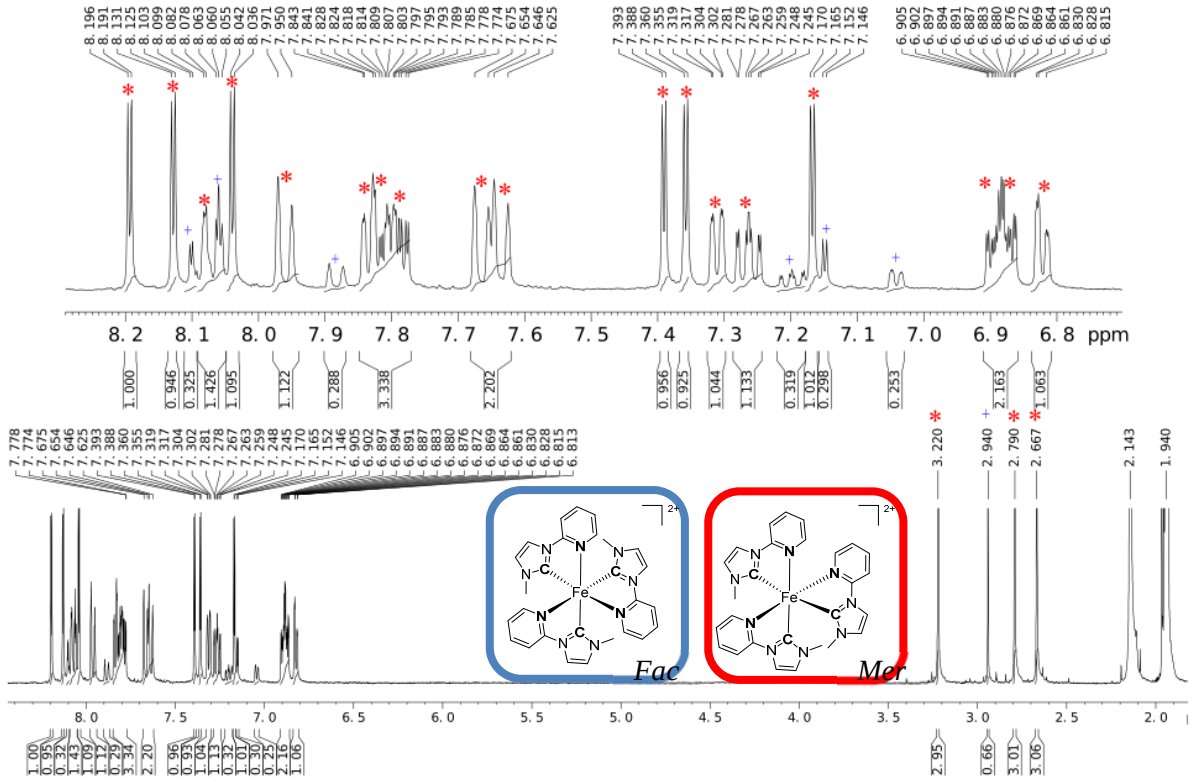

Figure S3. ^{1}H-NMR spectrum of the mixture *fac*-/*mer*-[Fe(MeImPy)$_3$](PF$_6$)$_2$ in CD$_3$CN.

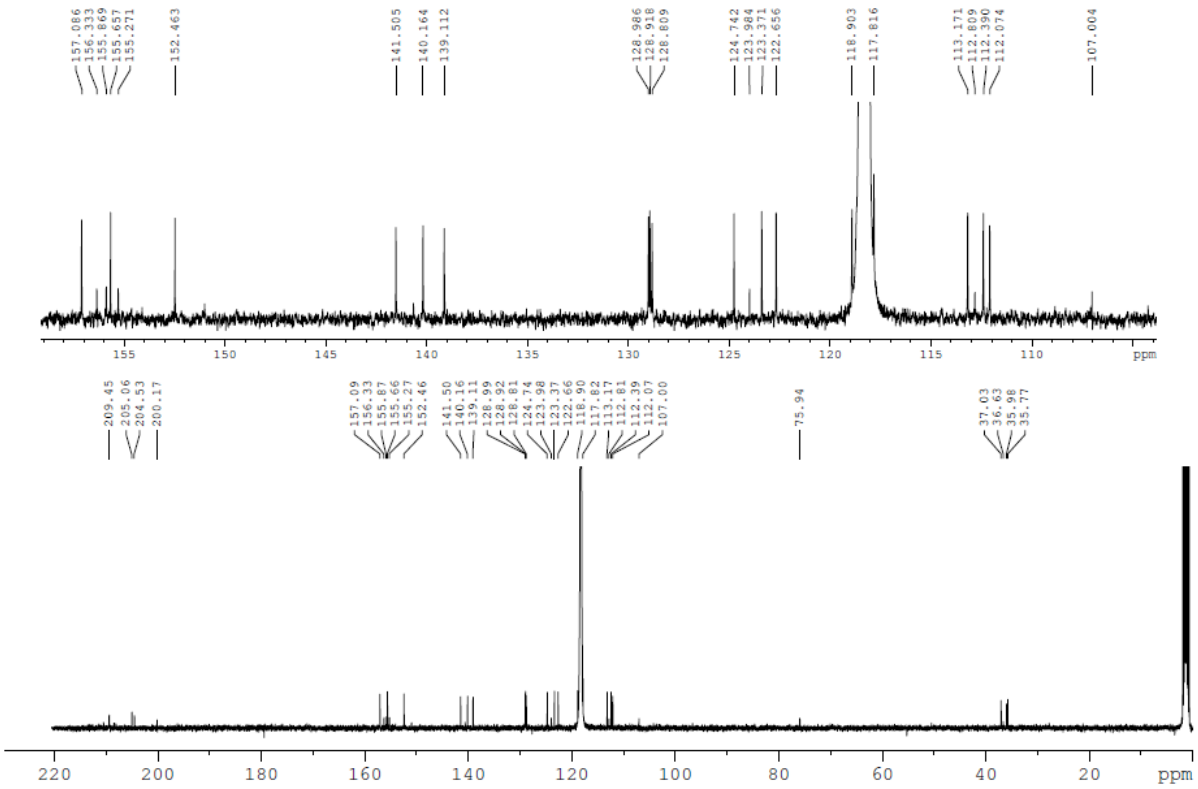

Figure S4. ^{13}C-NMR spectrum of the mixture *fac*-/*mer*-[Fe(MeImPy)$_3$](PF$_6$)$_2$ in CD$_3$CN.

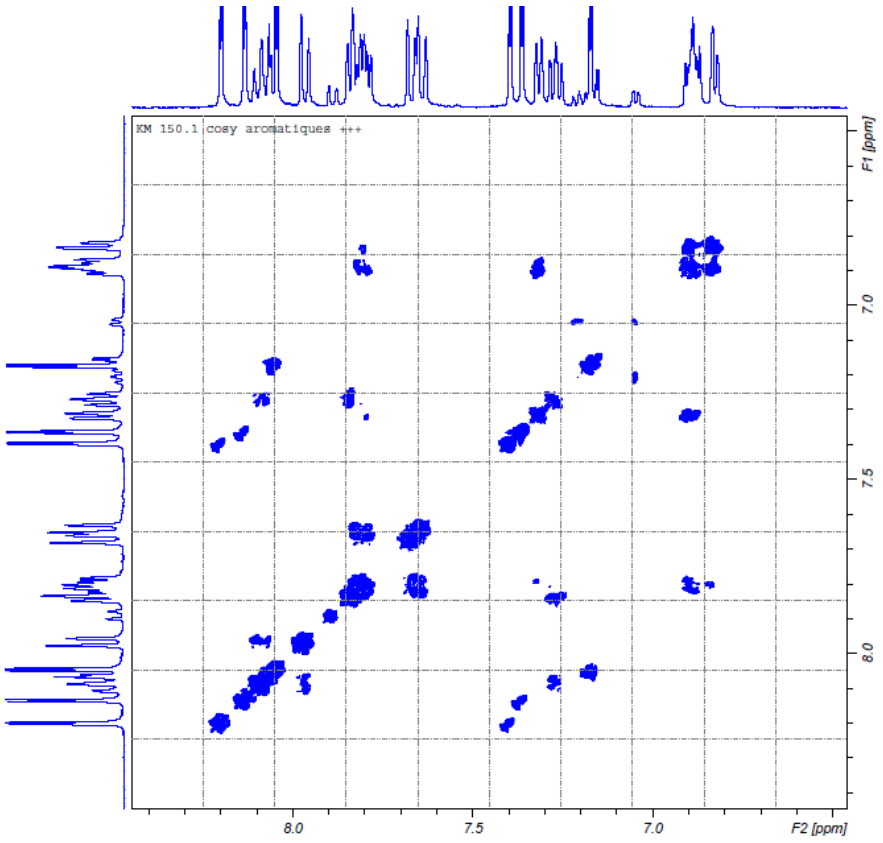

Figure S5. Aromatic region zoom of the COSY spectrum of the mixture *fac*-/*mer*-[Fe(MeImPy)$_3$](PF$_6$)$_2$ in CD$_3$CN.

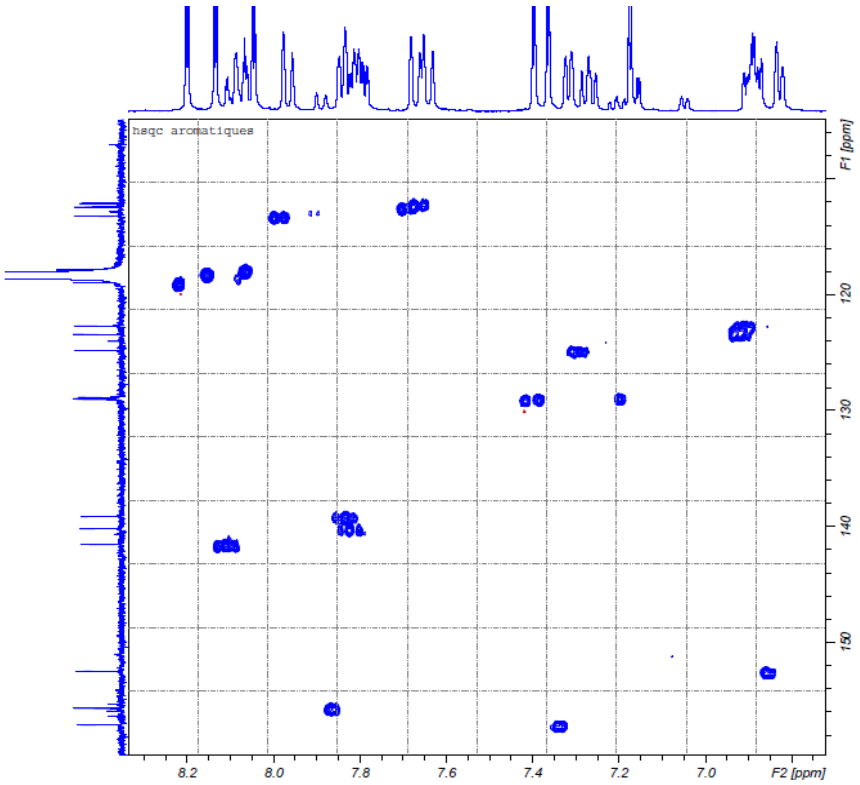

Figure S6. Aromatic region zoom of the HSQC spectrum of the mixture *fac*-/*mer*-[Fe(MeImPy)$_3$](PF$_6$)$_2$ in CD$_3$CN.

[Fe(N-(Et-Im-Py)$_3$](PF$_6$)$_2$, **C2 :**

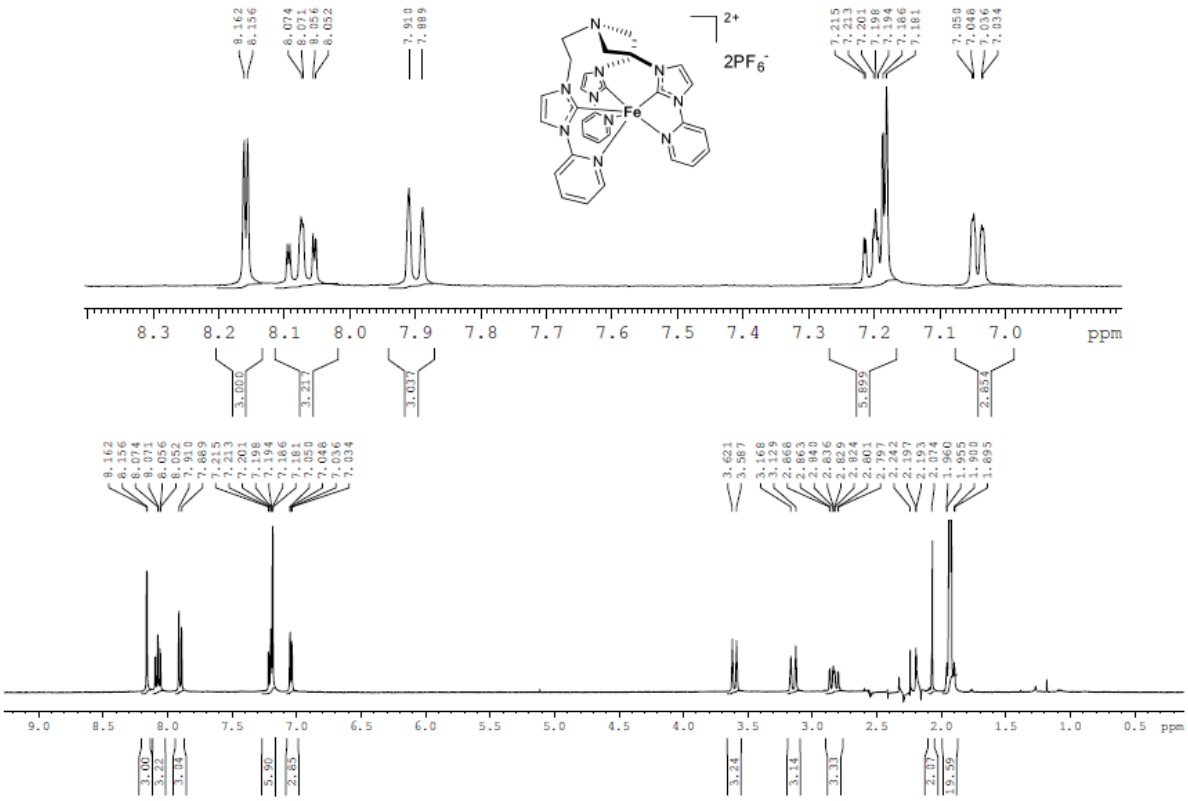

Figure S7. ^{1}H-NMR spectrum of the complex [Fe(N-(Et-Im-Py)$_3$](PF$_6$)$_2$ in CD$_3$CN.

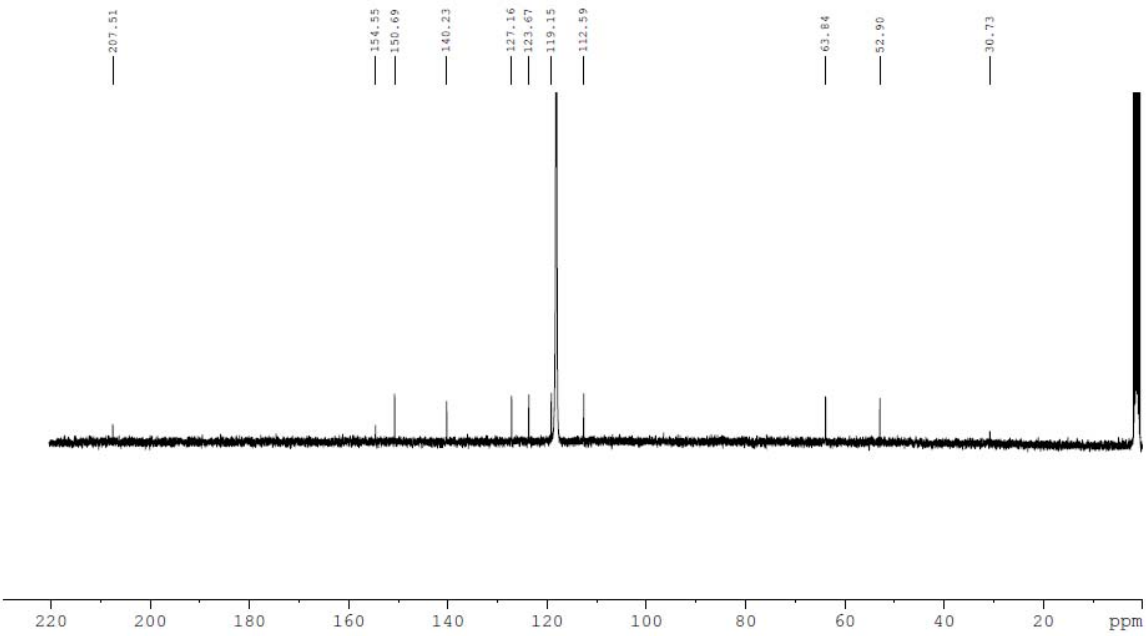

Figure S8. ^{13}C-NMR spectrum of the complex [Fe(N-(Et-Im-Py)$_3$](PF$_6$)$_2$ in CD$_3$CN.

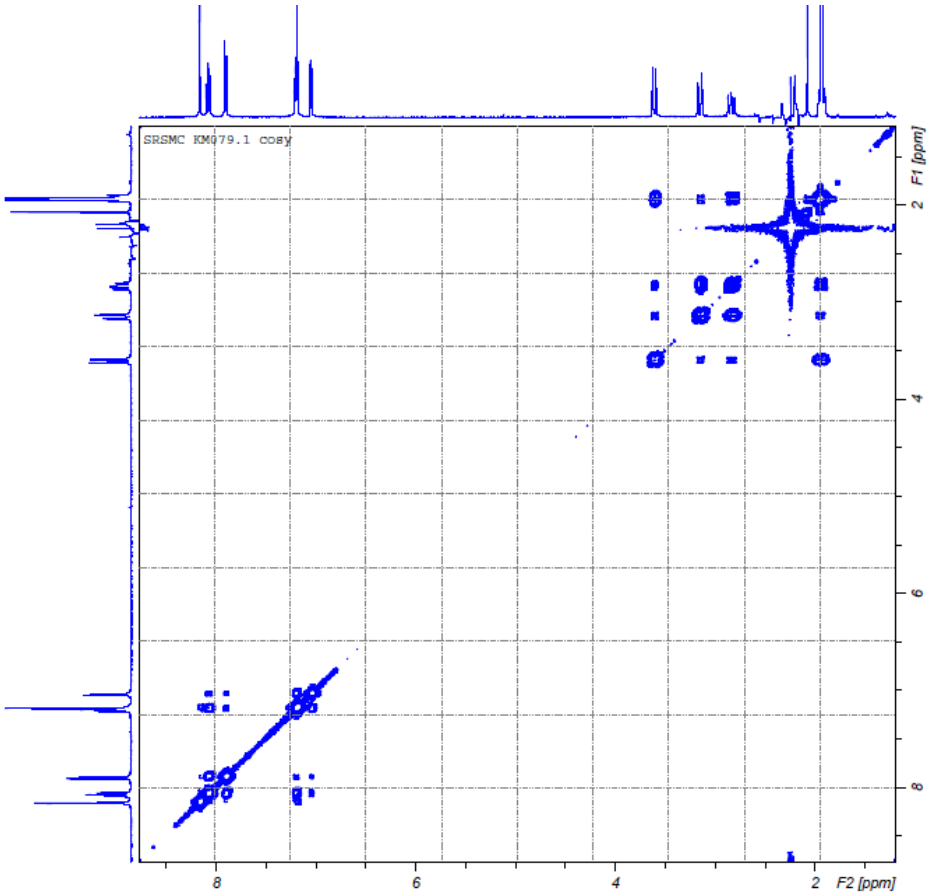

Figure S9. COSY spectrum of the complex [Fe(N-(Et-Im-Py)$_3$](PF$_6$)$_2$ in CD$_3$CN.

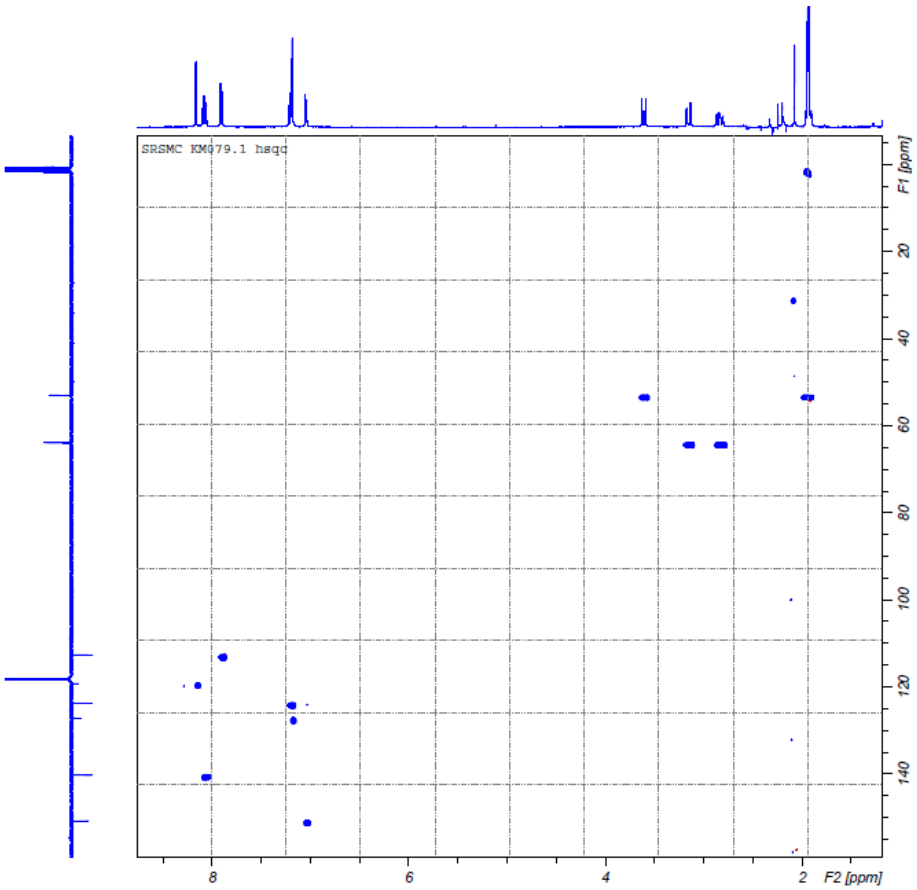

Figure S10. HSQC spectrum of the complex $[Fe(N\text{-}(Et\text{-}Im\text{-}Py)_3](PF_6)_2$ in CD_3CN

Cyclic Voltammetry

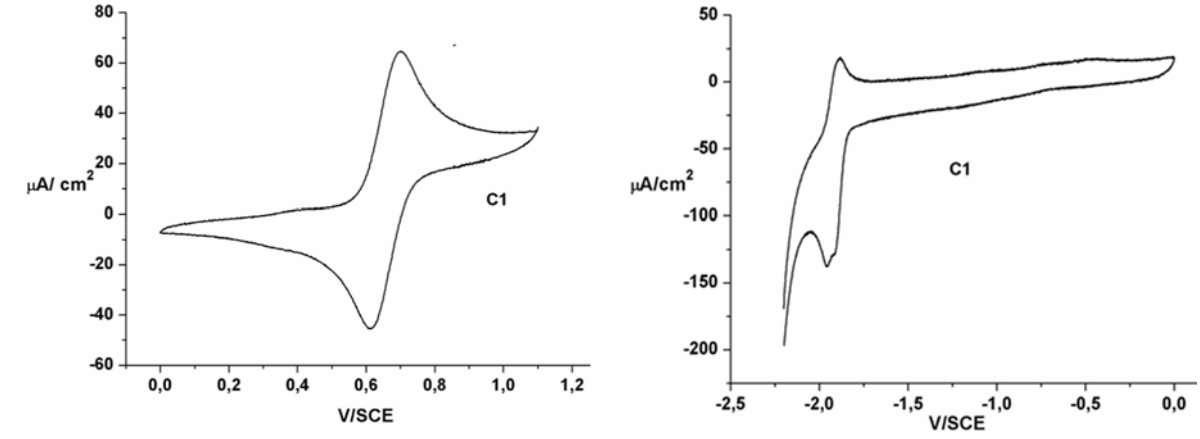

Figure S11. Cyclic voltammogram of **C1** in the positive (left) and negative (right) domain of potentials *vs* SCE.

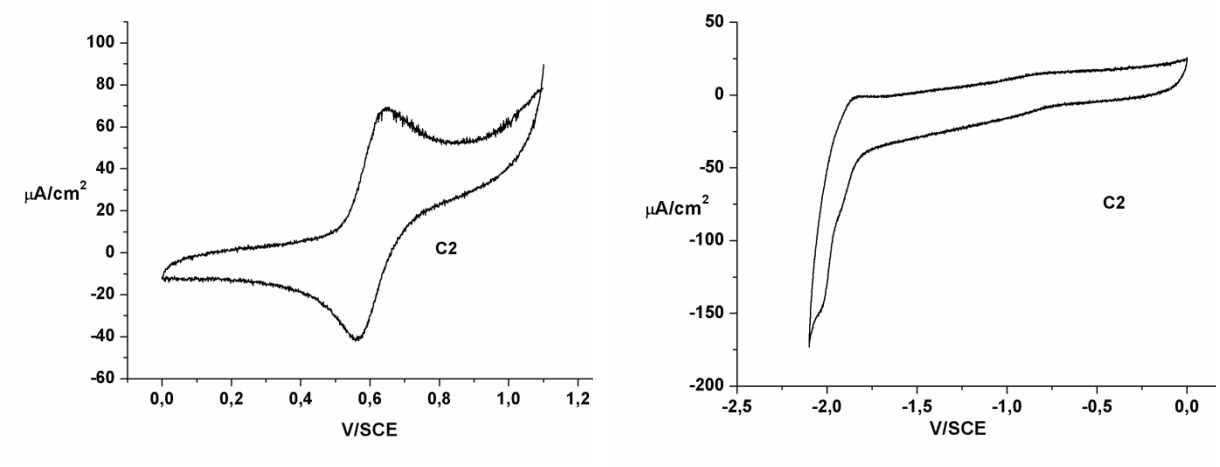

Figure S12. Cyclic voltammogram of **C2** in the positive (left) and negative (right) domain of potentials *vs* SCE.

Computations

Ground State structure of complexes

We have focused our analysis not only on the differences between tridentate (C0) vs bidentate (**C1** and **C2**) coordination, but also on the specific impact of the fac/mer isomerism on the Fe-N and the Fe-C bond lengths and the N-Fe-C bite angles. The data are summarised in Table S1.

The Fe-N bond lengths are slightly shorter for the tridentate complex C0 (1.948 Å) with respect to the bidentate compounds (>2.038 Å), whereas on the contrary the Fe-C distances are in general larger with respect to C1 and C2. Note that the tridentate coordination of C0 leads to a slightly smaller N-Fe-C bite angles as compared to the bidentate **C1** and **C2** complexes, even if the differences appear as marginal (less than 2°). As expected, the asymmetry of the *mer*-**C1** system give rise to non-equivalent bond lengths and angles, whereas the fac-C1 isomer and its **C2** analogue have much more symmetric values. For example, the Fe-N2 and Fe-C2 distances are clearly larger in mer-**C1** with respect to the rest of Fe-N and Fe-C bond lengths, leading to a N2-Fe-C2 angle of 79.23°, the smallest within the bidentate compounds studied in this work.

Table S1. Optimized Fe-N and Fe-C distances (Å), and N-Fe-C bite angles (º) for **C1** and **C2** at their ground-state equilibrium geometry, using very tight convergence thresholds.

Bond/angle	**C0**	*mer*-**C1**	*fac*-**C1**	**C2**
Fe-N1	1.948	2.038	2.073	2.070
Fe-N2	1.948	2.082	2.072	2.068
Fe-N3	-	2.042	2.070	2.070
Fe-C1	1.995	1.942	1.949	1.947
Fe-C2	1.985	1.992	1.950	1.948
Fe-C3	1.995	1.983	1.947	1.947
Fe-C4	1.985	-	-	-
N1-Fe-C1	79.08	80.51	80.00	80.21
N1-Fe-C2	79.06	-	-	-
N2-Fe-C2	-	79.23	80.03	80.24
N2-Fe-C3	79.09	-	-	-
N2-Fe-C4	79.06	-	-	-
N3-Fe-C3	-	79.90	80.01	80.21

Computed UV-Vis spectrum of C2

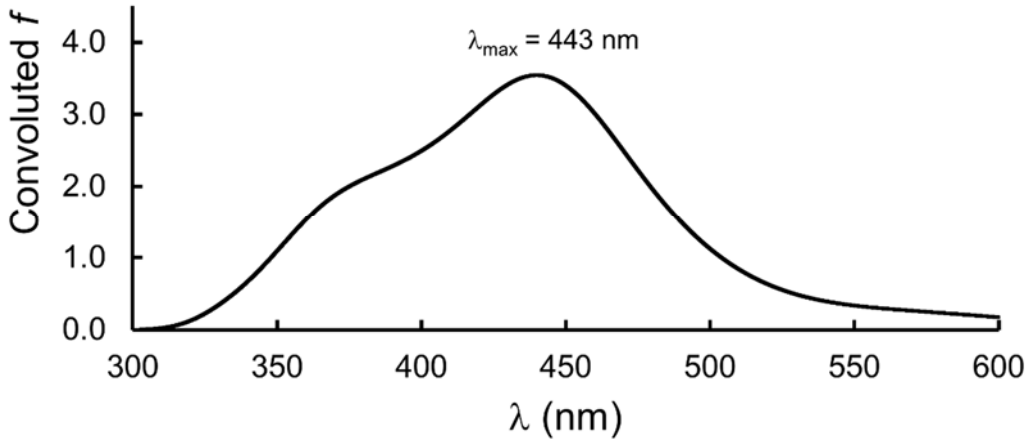

Figure S13. UV-Vis absorption spectrum of **C2** computed with the TD-DFT/HCTH method. The spectrum has been obtained as a convolution of the first 30 singlet excitation energies of 20 different structures obtained with a semiclassical Wigner distribution of the S_0 minimum geometry at room temperature. The energies have been blue-shifted 0.28 eV for an easier visual comparison with the experimental recordings.

Natural transition orbitals

State	oNTO		vNTO	Weight (%)
S_{10} λ = 443 nm (*f* = 0.058)		MLCT	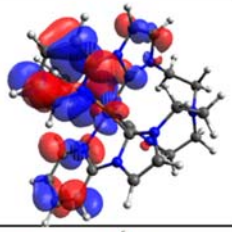	49
S_{10} λ = 443 nm (*f* = 0.051)	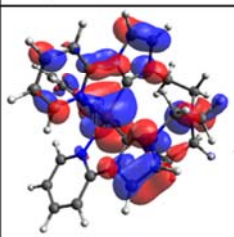	MLCT	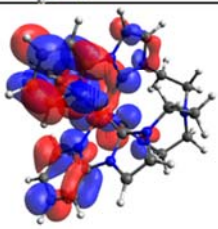	33
S_{11} λ = 443 nm (*f* = 0.059)	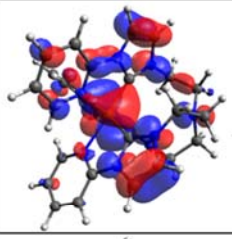	MLCT	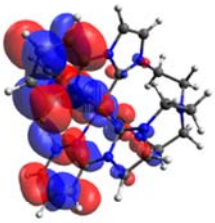	48
S_{11} λ = 443 nm (*f* = 0.059)	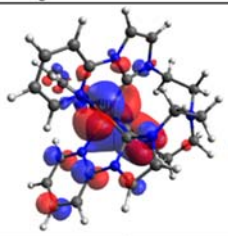	MLCT	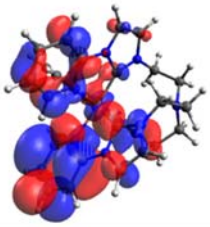	33
S_{15} λ = 429 nm (*f* = 0.070)	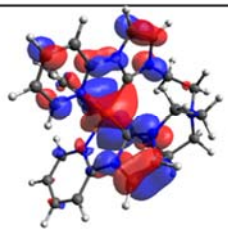	MLCT	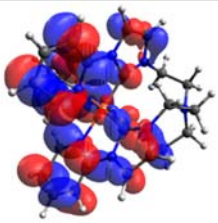	77
S_{16} λ = 429 nm (*f* = 0.071)	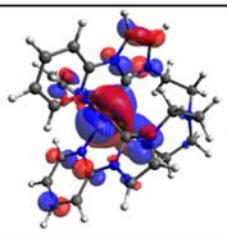	MLCT	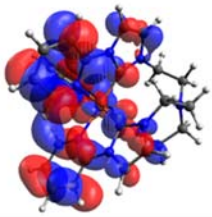	73

Figure S14. Occupied or hole (oNTO) and virtual (vNTO) isosurfaces for the bright ^{1}MLCT states of **C2** at the S_0 min geometry. The rest of oNTO → vNTO couples (not shown) are of ^{1}MLCT nature as well

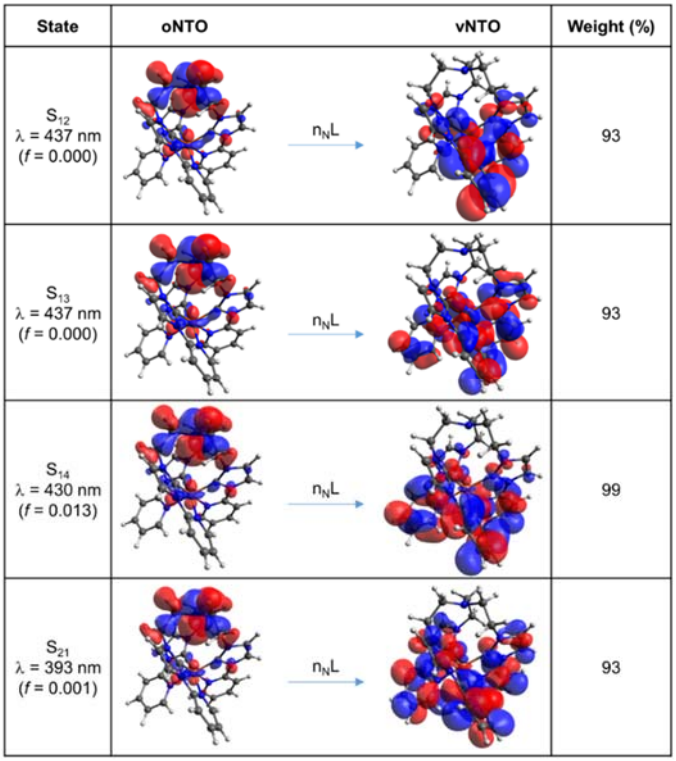

Figure S15. Occupied or hole (oNTO) and virtual (vNTO) isosurfaces for some dark ^1n_NL states of **C2** at the S_0 min geometry.

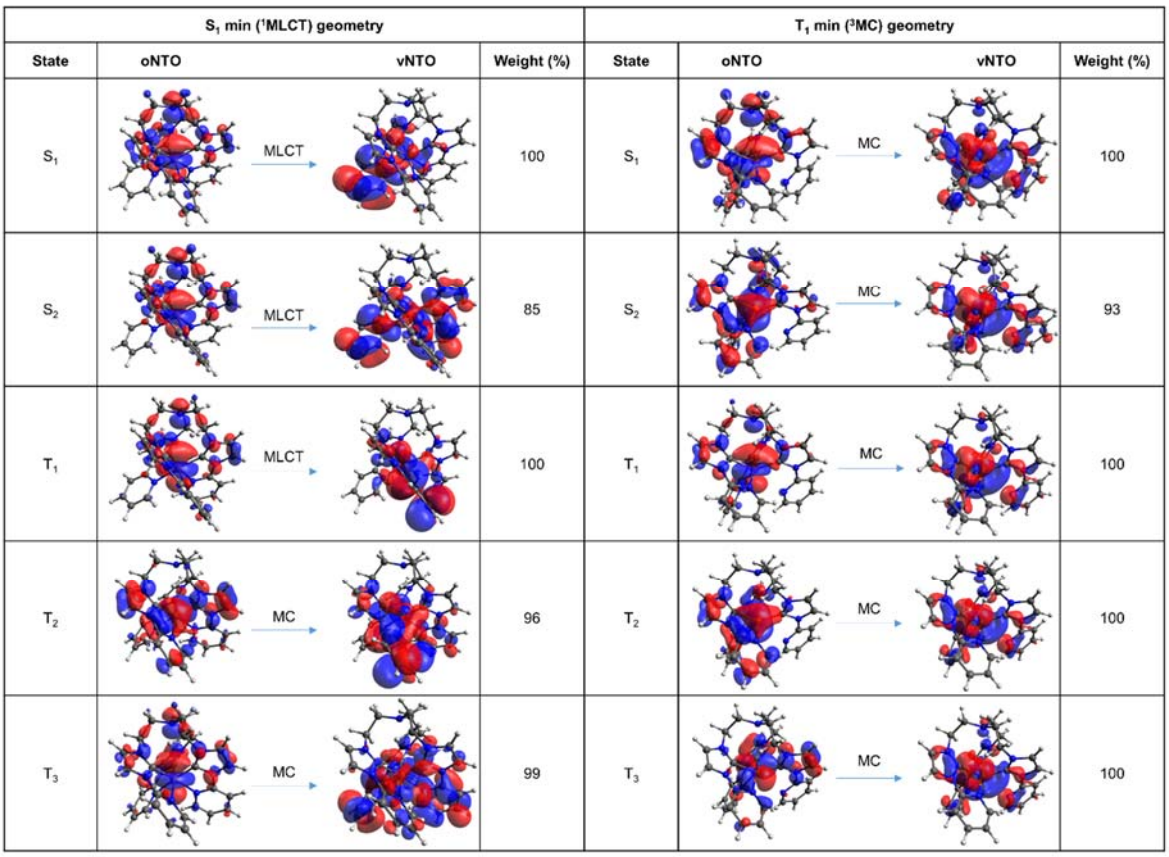

Figure S16. Occupied or hole (oNTO) and virtual (vNTO) isosurfaces for the S_1, S_2, T_1, T_2 and T_3 states of **C2** at the S_1 (^{1}MLCT) min and T_1 (^{3}MC) min geometries.

Fe-C and Fe-N bond lengths of C2 at different states

Table S2. Fe-C and Fe-N bond lengths (Å) of **C2** at the S_1 (^{1}MLCT), T_1 (^{3}MC), T_2 (^{3}MC) and Q_1 optimized geometries.

Bond	C2
S_1 (^{1}MLCT) min	
Fe – N1	2.130
Fe – N2	2.069
Fe – N3	2.110
Fe – C1	1.896
Fe – C2	1.942
Fe – C3	1.915
T_1 (^{3}MC) min	
Fe – N1	2.820
Fe – N2	2.164
Fe – N3	2.044
Fe – C1	1.899
Fe – C2	1.982
Fe – C3	2.036
T_2 (^{3}MC) min	
Fe – N1	2.725
Fe – N2	2.120
Fe – N3	2.060
Fe – C1	1.923
Fe – C2	1.949
Fe – C3	2.002
Q_1 min	
Fe – N1	2.366
Fe – N2	2.390
Fe – N3	2.398
Fe – C1	2.149
Fe – C2	2.131
Fe – C3	2.141

Simulated triplet-triplet transient absorption spectra

Computational details. All excited-state absorption (ESA) spectra have been obtained using the pure BLYP functional in combination with the 6-31G basis set as implemented in the TERACHEM software package. No solvent effects have been included. For the triplet transient absorptions, the T_1 state computed with the unrestricted (u)DFT method has been used as the reference state for further time-dependent (TD-)uDFT calculations. On the other hand, the transient singlet absorptions have been computed with the restricted DFT ansatz, in which the excitations are obtained using the S_0 state as the reference state. Oscillator strengths have been computed using the formula $f = {}^2/_3\,\Delta E_{i\to f}\,TDM^2$, where $\Delta E_{i\to f}$ stands for the energy difference between the initial (i) and final (f) states, and TDM refers to the transition dipole moment between the excited states. 40 excited states have been computed for all geometries. The obtained excitations have been convoluted using Gaussian functions with an amplitude of 0.1. In the case of triplet states, the expectation values of the $\hat{S}^2$ operator, $\langle\hat{S}^2\rangle$, are between 2 and 3 in the majority of cases, indicating thus reasonably low spin contamination due to the mixing with higher-spin quintet states.

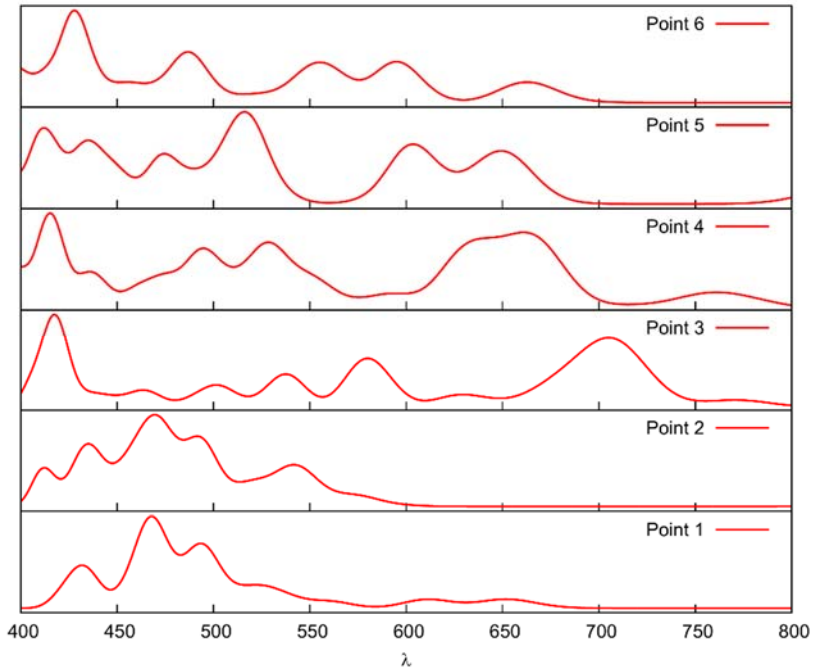

Figure S17. $T_1 \rightarrow T_X$ absorptions at different regions of the PES of **C2** (*fac*-only) displayed in Figure 4 of the main text. The Fe-N1 distances (in Å) for the points are the following: Point 1 (2.079), Point 2 (2.130), Point 3 (2.569), Point 4 (2.820), Point 5 (3.048), Point 6 (3.598).

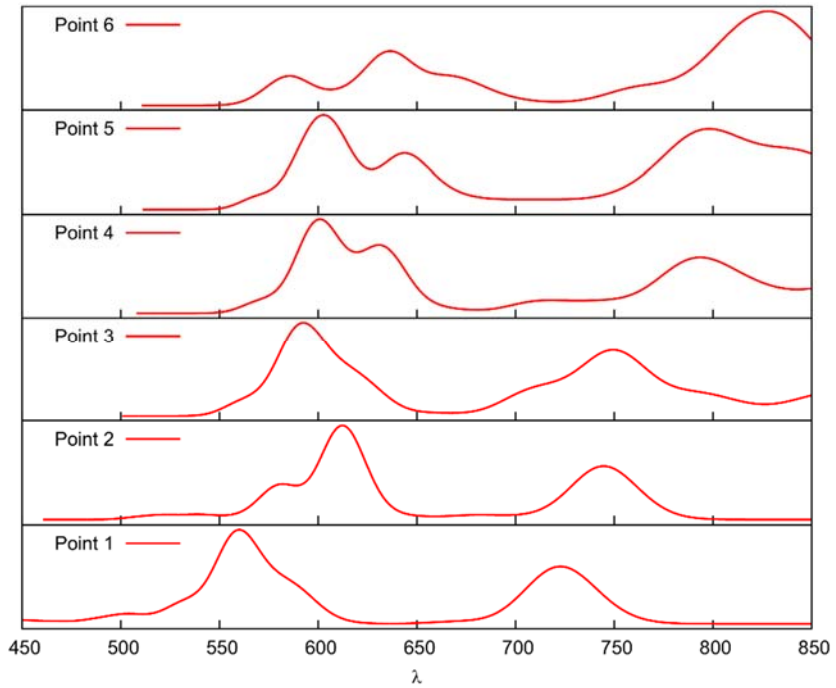

Figure S18. $T_2 \rightarrow T_X$ absorptions at different regions of the PES of **C2** (*fac*-only) displayed in Figure 4 of the main text. The Fe-N1 distances (in Å) for the points are the following: Point 1 (2.079), Point 2 (2.130), Point 3 (2.569), Point 4 (2.820), Point 5 (3.048), Point 6 (3.598).

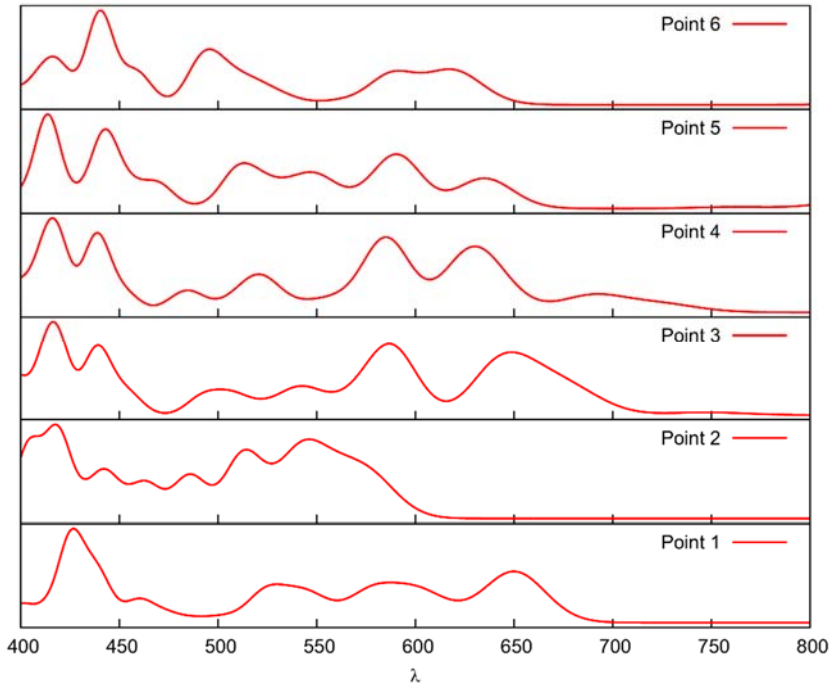

Figure S19. $T_1 \rightarrow T_X$ absorptions at different regions of the PES of *mer*-**C1** displayed in Figure 7 of reference 23 of the main text (A. Francés-Monerris *et al*, *Inorg. Chem.* 2018, **57**, 10431-10441). The Fe-N1 distances (in Å) for the points are the following: Point 1 (2.082), Point 2 (2.147), Point 3 (2.443), Point 4 (2.526), Point 5 (2.781), Point 6 (2.981).

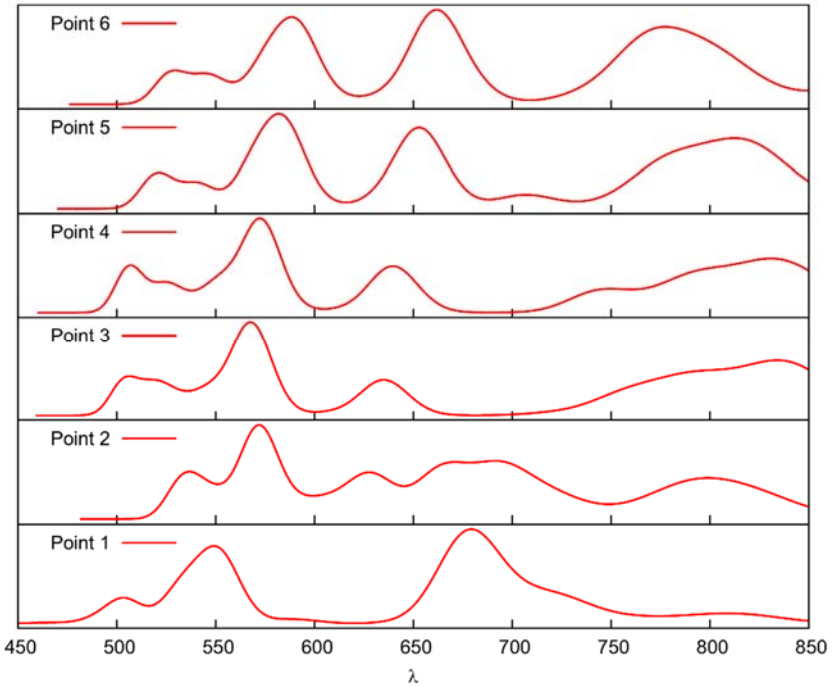

Figure S20. $T_2 \rightarrow T_X$ absorptions at different regions of the PES of *mer*-**C1** displayed in Figure 7 of reference 23 of the main text (A. Francés-Monerris *et al*, *Inorg. Chem.* 2018, **57**, 10431-10441). The Fe-N1 distances (in Å) for the points are the following: Point 1 (2.082), Point 2 (2.147), Point 3 (2.443), Point 4 (2.526), Point 5 (2.781), Point 6 (2.981).

Cartesian coordinates of the relevant geometries of C2

S_0 min (very tight convergence thresholds)

C	1.749619	3.640054	0.052713
C	0.747087	3.811535	0.944147
N	0.036616	2.611767	0.942891
C	0.581948	1.686409	0.069568
N	1.633676	2.350163	-0.475507
H	2.527411	4.317565	-0.262192
H	0.482411	4.663532	1.547572
N	-1.529876	1.003651	1.403021
C	-1.092821	2.248181	1.687249
C	-1.699535	3.084150	2.624489
C	-2.611979	0.555524	2.071803
H	-1.312082	4.076006	2.819820
C	-2.816417	2.603415	3.301679
C	-3.282688	1.316378	3.021851
H	-3.313823	3.226550	4.037077
H	-4.148830	0.904683	3.526334
C	1.746851	-1.789216	-3.174838
H	-2.944824	-0.444307	1.824899
Fe	-0.386953	-0.000639	-0.000740
C	0.743574	-1.105434	-3.770607
N	0.038687	-0.496683	-2.733083
C	0.586371	-0.783374	-1.494484
N	1.636462	-1.590467	-1.794644
N	-1.528671	0.708642	-1.574970
C	-1.087446	0.333691	-2.793568
C	-1.685284	0.734233	-3.988368
C	-2.609426	1.513798	-1.524541
C	-2.800173	1.564064	-3.914144
C	-3.272986	1.961239	-2.660718
H	2.520488	-2.407100	-3.602542
H	0.473482	-1.018017	-4.809588
H	-1.291313	0.411424	-4.943753
H	-2.946325	1.797221	-0.535908
H	-3.290718	1.895067	-4.823183
H	-4.138189	2.605680	-2.559186
C	1.755366	-1.852452	3.131688
C	0.753675	-2.712089	2.837648
N	0.044310	-2.116990	1.795423
C	0.588751	-0.899196	1.425317
N	1.639983	-0.754522	2.272770
N	-1.521348	-1.721822	0.169749
C	-1.083349	-2.585186	1.109425
C	-1.687740	-3.815142	1.369276
C	-2.600719	-2.082568	-0.553947
C	-2.802698	-4.166705	0.614005
C	-3.268903	-3.286527	-0.365966
H	2.531962	-1.914791	3.877521
H	0.489593	-3.659180	3.277210
H	-1.300830	-4.476047	2.134636
H	-2.932780	-1.372219	-1.299973
H	-3.298559	-5.115300	0.789617
H	-4.133210	-3.522801	-0.975342

C	2.619145	-2.149465	-0.859761
H	2.126446	-2.320687	0.094189
C	3.864181	-1.260951	-0.684411
H	2.924780	-3.121955	-1.256376
N	3.624464	0.003581	-0.003519
H	4.292503	-1.064304	-1.673952
H	4.604158	-1.862519	-0.136578
C	2.620797	0.336367	2.290071
H	2.926904	0.478289	3.330569
C	2.612842	1.823859	-1.432843
H	2.915297	2.655705	-2.075579
C	3.861028	1.225872	-0.758720
H	2.117704	1.084948	-2.057989
H	2.126846	1.247845	1.962866
H	4.293913	1.983747	-0.095808
H	4.596008	1.051768	-1.558037
C	3.865629	0.047034	1.431842
H	4.603797	0.824164	1.677976
H	4.296900	-0.907043	1.756097

S_1 (^{1}MLCT) min

C	1.645110	3.675990	-0.056398
C	0.648276	3.817586	0.856965
N	0.004917	2.597560	0.916906
C	0.567318	1.699342	0.051956
N	1.581398	2.383971	-0.548047
H	2.378339	4.386925	-0.405967
H	0.343849	4.677728	1.431298
N	-1.602818	0.996727	1.305532
C	-1.064565	2.187125	1.739319
C	-1.497108	2.888223	2.844374
C	-2.626431	0.495672	2.076173
H	-1.023908	3.825223	3.119929
C	-2.561895	2.371763	3.607021
C	-3.123179	1.137119	3.186593
H	-2.921433	2.893229	4.486385
H	-3.955605	0.688657	3.721835
C	1.700239	-1.901521	-3.179416
H	-3.067196	-0.434813	1.736873
Fe	-0.316271	-0.026810	-0.048085
C	0.713095	-1.204863	-3.793651
N	0.042663	-0.537141	-2.784453
C	0.585116	-0.808629	-1.545533
N	1.608112	-1.658933	-1.815552
N	-1.453294	0.751106	-1.646677
C	-1.045636	0.335272	-2.859628
C	-1.642560	0.737831	-4.053500
C	-2.494385	1.600955	-1.587906
C	-2.718360	1.614643	-3.974578
C	-3.154430	2.053226	-2.723008
H	2.453471	-2.553340	-3.595570
H	0.440434	-1.149896	-4.835237
H	-1.281495	0.382292	-5.011152
H	-2.794912	1.908212	-0.593373
H	-3.208769	1.951020	-4.883441
H	-3.991073	2.736505	-2.621389

C	1.597827	-1.681361	3.245564
C	0.600919	-2.552697	2.961374
N	-0.033570	-2.041803	1.842888
C	0.540725	-0.856373	1.425481
N	1.549088	-0.652430	2.313661
N	-1.456873	-1.747455	0.091104
C	-1.112681	-2.544602	1.122197
C	-1.765906	-3.740197	1.421755
C	-2.487053	-2.134621	-0.685294
C	-2.825725	-4.122502	0.609616
C	-3.195141	-3.306649	-0.462201
H	2.333116	-1.701643	4.035505
H	0.300704	-3.459147	3.461026
H	-1.460831	-4.350956	2.263164
H	-2.751965	-1.476873	-1.503473
H	-3.357543	-5.047197	0.813391
H	-4.017961	-3.568565	-1.118733
C	2.602599	-2.167928	-0.876528
H	2.116178	-2.363878	0.075350
C	3.819739	-1.241279	-0.701889
H	2.951089	-3.127835	-1.266853
N	3.571528	0.010519	-0.014582
H	4.239774	-1.035083	-1.691809
H	4.574474	-1.833686	-0.165059
C	2.569652	0.391222	2.284216
H	2.907434	0.533972	3.314198
C	2.591561	1.857209	-1.457665
H	2.941447	2.694164	-2.068242
C	3.809830	1.238929	-0.749187
H	2.124126	1.144932	-2.132503
H	2.111924	1.322861	1.965002
H	4.227157	1.990245	-0.070574
H	4.565049	1.077274	-1.531523
C	3.791948	0.039855	1.418738
H	4.564919	0.779171	1.674577
H	4.176592	-0.931445	1.746347

T_1 (^{3}MC) min

C	1.462913	3.761965	0.285719
C	0.478421	3.818925	1.213942
N	-0.168560	2.590332	1.177561
C	0.396009	1.762369	0.233879
N	1.398842	2.509307	-0.303318
H	2.181448	4.507903	-0.019280
H	0.164183	4.632303	1.847812
N	-2.059598	1.283625	1.539185
C	-1.243030	2.212501	2.030227
C	-1.390535	2.786816	3.297418
C	-3.083661	0.884368	2.303116
H	-0.683082	3.512894	3.682230
C	-2.471119	2.371856	4.071490
C	-3.341946	1.403645	3.570201
H	-2.619596	2.794805	5.061351
H	-4.194222	1.055025	4.145432
C	1.980239	-2.168058	-3.364062
H	-3.728933	0.120073	1.872183
Fe	-0.134749	-0.080778	-0.267031

C	0.923753	-1.578021	-3.978823
N	0.233406	-0.914089	-2.979263
C	0.824521	-1.087921	-1.745834
N	1.903155	-1.863057	-2.013716
N	-1.134609	0.581377	-1.911263
C	-0.842904	-0.027420	-3.083993
C	-1.528605	0.224519	-4.270986
C	-2.134305	1.490307	-1.912162
C	-2.554543	1.163176	-4.250603
C	-2.859154	1.810811	-3.050982
H	2.770764	-2.778550	-3.774596
H	0.628043	-1.583872	-5.015568
H	-1.272718	-0.298064	-5.185327
H	-2.350017	1.951068	-0.955330
H	-3.106632	1.382991	-5.159587
H	-3.649018	2.552468	-2.990857
C	1.584765	-1.746099	3.137084
C	0.531992	-2.554235	2.872882
N	-0.077877	-2.024567	1.746317
C	0.582612	-0.892064	1.289813
N	1.601292	-0.735732	2.184400
N	-1.587515	-1.642876	0.076208
C	-1.233638	-2.448309	1.095502
C	-1.957742	-3.585122	1.463281
C	-2.706890	-1.947944	-0.604685
C	-3.109374	-3.883705	0.745758
C	-3.497834	-3.048944	-0.305303
H	2.316626	-1.796892	3.929086
H	0.174841	-3.427226	3.394217
H	-1.636605	-4.216951	2.282864
H	-2.975940	-1.279090	-1.414480
H	-3.697327	-4.758982	1.006889
H	-4.393895	-3.244376	-0.885151
C	2.980655	-2.163996	-1.078368
H	2.544765	-2.416638	-0.111929
C	3.991137	-1.007874	-0.953671
H	3.497360	-3.052010	-1.451299
N	3.532511	0.120105	-0.160346
H	4.242284	-0.667606	-1.962749
H	4.915025	-1.438500	-0.536090
C	2.629504	0.300787	2.191379
H	3.003722	0.365074	3.216704
C	2.361452	2.066553	-1.311298
H	2.632275	2.948591	-1.899121
C	3.653924	1.445403	-0.749689
H	1.856774	1.370165	-1.978593
H	2.164484	1.257316	1.965468
H	4.078889	2.139512	-0.014479
H	4.363316	1.427140	-1.588508
C	3.814886	0.022962	1.262383
H	4.614833	0.722191	1.557658
H	4.191717	-0.979557	1.486342

T_2 (^{3}MLCT) min

C	1.557203	3.679808	0.199682
C	0.574358	3.784093	1.126276

N	-0.095887	2.570092	1.120181
C	0.454508	1.696110	0.204115
N	1.475636	2.410515	-0.350752
H	2.288273	4.404122	-0.126869
H	0.278956	4.621177	1.738242
N	-1.962721	1.249960	1.484530
C	-1.181126	2.219165	1.960938
C	-1.378039	2.838014	3.198945
C	-2.997417	0.852935	2.237614
H	-0.700107	3.598063	3.570951
C	-2.467826	2.424790	3.961000
C	-3.299299	1.413834	3.476025
H	-2.654301	2.882006	4.928847
H	-4.158186	1.066182	4.041889
C	1.955627	-1.950645	-3.324283
H	-3.613658	0.059122	1.819306
Fe	-0.287368	-0.054494	-0.224177
C	0.944025	-1.296745	-3.947494
N	0.203953	-0.705466	-2.937737
C	0.729728	-0.972365	-1.683731
N	1.813136	-1.741380	-1.960500
N	-1.330749	0.624692	-1.865295
C	-0.915741	0.130288	-3.048835
C	-1.541610	0.429769	-4.257373
C	-2.394515	1.448639	-1.855888
C	-2.640847	1.283632	-4.231138
C	-3.076733	1.804423	-3.013257
H	2.757113	-2.544885	-3.737550
H	0.710768	-1.213720	-4.996675
H	-1.190852	0.009560	-5.192341
H	-2.690978	1.820241	-0.881545
H	-3.148430	1.536362	-5.157589
H	-3.925973	2.476819	-2.952945
C	1.596283	-1.690721	3.145455
C	0.542476	-2.506392	2.909614
N	-0.091086	-1.988535	1.793761
C	0.546588	-0.850594	1.315337
N	1.586974	-0.687541	2.187472
N	-1.615020	-1.668804	0.128062
C	-1.216452	-2.476963	1.129852
C	-1.852352	-3.675292	1.454651
C	-2.692204	-2.049259	-0.587209
C	-2.967195	-4.045670	0.709846
C	-3.397206	-3.216870	-0.329945
H	2.341894	-1.729072	3.925069
H	0.196977	-3.373243	3.448574
H	-1.491420	-4.304693	2.259721
H	-3.000759	-1.383374	-1.385038
H	-3.490072	-4.969532	0.939234
H	-4.266616	-3.463602	-0.930649
C	2.825313	-2.174881	-1.002835
H	2.334799	-2.384724	-0.054080
C	3.965132	-1.152598	-0.828430
H	3.244491	-3.114759	-1.373871
N	3.621666	0.052754	-0.104166
H	4.343376	-0.887753	-1.821923
H	4.782897	-1.691160	-0.324915

C	2.616073	0.349204	2.194235
H	2.947790	0.453250	3.231476
C	2.438171	1.938883	-1.346701
H	2.709464	2.805313	-1.957593
C	3.735283	1.328172	-0.780159
H	1.933992	1.229810	-1.997089
H	2.163733	1.295417	1.913379
H	4.196835	2.060428	-0.105208
H	4.414098	1.243169	-1.641135
C	3.842053	0.041886	1.325261
H	4.608867	0.780940	1.612739
H	4.235405	-0.935808	1.622280

Q_1 min

C	1.737309	3.965196	0.216804
C	0.661964	4.080930	1.033342
N	0.023419	2.841231	1.005581
C	0.683349	1.956687	0.186959
N	1.729771	2.666924	-0.288879
H	2.491614	4.687556	-0.053242
H	0.308495	4.926514	1.598146
N	-1.593365	1.228398	1.456049
C	-1.147511	2.465897	1.714346
C	-1.769556	3.332894	2.616340
C	-2.695000	0.808523	2.102243
H	-1.378963	4.323371	2.810150
C	-2.912729	2.883530	3.272392
C	-3.390126	1.596922	3.013970
H	-3.419628	3.532749	3.978480
H	-4.275658	1.210128	3.504846
C	1.769429	-1.831984	-3.534891
H	-3.023978	-0.198246	1.870198
Fe	-0.148958	-0.006975	-0.005627
C	0.682289	-1.208862	-4.052487
N	0.035206	-0.610379	-2.972649
C	0.696112	-0.852626	-1.791847
N	1.755466	-1.605020	-2.160454
N	-1.593856	0.582981	-1.815148
C	-1.133146	0.196377	-3.013026
C	-1.734386	0.562754	-4.218734
C	-2.683436	1.368588	-1.778792
C	-2.868435	1.370436	-4.163488
C	-3.356627	1.786023	-2.923231
H	2.535163	-2.418952	-4.017225
H	0.325529	-1.165381	-5.067513
H	-1.334108	0.241277	-5.171448
H	-3.020947	1.661272	-0.790708
H	-3.359478	1.672755	-5.082469
H	-4.234567	2.416063	-2.840497
C	1.782945	-2.166675	3.301848
C	0.697281	-2.924676	3.020842
N	0.029869	-2.267389	1.984853
C	0.680396	-1.110756	1.617473
N	1.750779	-1.066902	2.442750
N	-1.579390	-1.854942	0.361369
C	-1.144292	-2.688816	1.318599

C	-1.786519	-3.888916	1.635823
C	-2.683255	-2.200097	-0.325495
C	-2.929703	-4.228686	0.917630
C	-3.391468	-3.372577	-0.085023
H	2.561007	-2.303818	4.036306
H	0.353734	-3.840208	3.471149
H	-1.411043	-4.542459	2.412482
H	-3.000749	-1.500990	-1.090565
H	-3.450940	-5.153785	1.140318
H	-4.276633	-3.603510	-0.666118
C	2.826860	-2.057673	-1.262630
H	2.371661	-2.371239	-0.322507
C	3.895427	-0.977285	-1.024844
H	3.283872	-2.933128	-1.729320
N	3.511942	0.013202	-0.010749
H	4.083681	-0.467879	-1.974408
H	4.835710	-1.481833	-0.752212
C	2.814588	-0.055578	2.404795
H	3.265452	-0.029990	3.399573
C	2.795587	2.138041	-1.151617
H	3.238074	2.992473	-1.668300
C	3.882325	1.390103	-0.361631
H	2.339430	1.489660	-1.900638
H	2.355252	0.915740	2.216694
H	4.087766	1.952387	0.554074
H	4.810261	1.414035	-0.954233
C	3.894275	-0.367073	1.355364
H	4.824493	0.136514	1.662156
H	4.101842	-1.440719	1.386342

Photophysics

Analysis of spectra and kinetic traces of C2

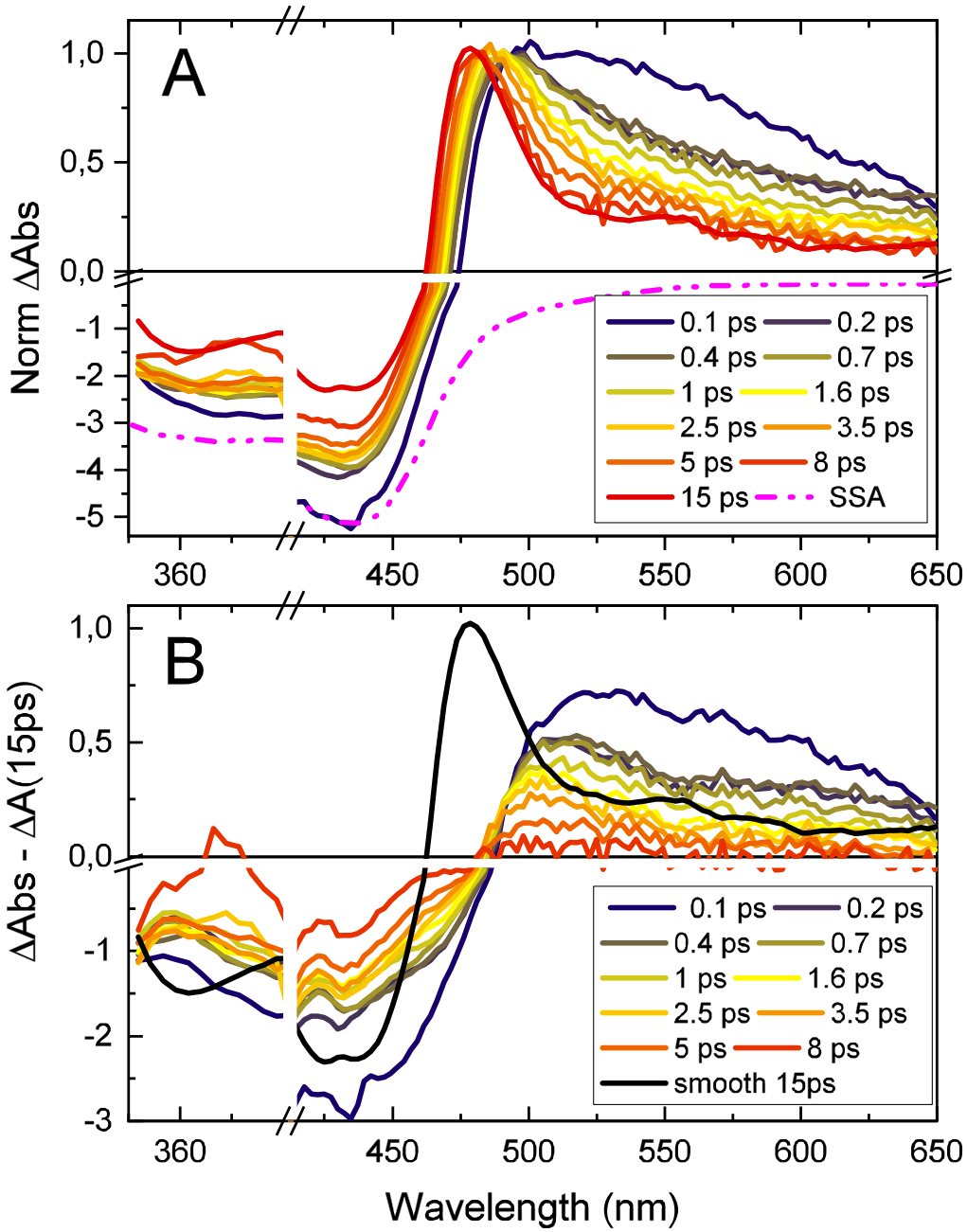

Figure S21 Selected spectra of **C2** in AcN at different times normalized on the maximum of ESA band (A). The inverted steady-state absorption spectrum is shown for comparison (dash-dotted line). Spectra minus the smoothed spectrum at 15 ps in the bottom (B). Note the different scaling of positive and negative ΔA.

In Fig. S21 the spectra at selected times are normalized on the ESA band. This operation does not change its shape but underlines the spectral narrowing in the first picoseconds. In addition, during this period, the GSB remains almost constant until 3-5 ps. The minor band of the GSB (<380 nm), does not have any time evolutions for all the spectra selected, indicating the presence of an ESA in this range, the decay of which seems to compensate the GSB recovery. The shift, in the region 462-472 nm, is still observed and no clear isosbestic point is identified. For delays longer than 15 ps the signal decays in

ESA and GSB due to the 15-20 ps component without further spectral evolution. We then subtract the smoothed and normalized 15 ps spectrum, from the earlier delay spectra, and the result given in Fig. S21 bottom panel (B). The remaining ESA band decays homogenously for all the wavelengths > 485 nm after 0.2 ps, with this long-wavelength portion almost constant in shape. A quasi-isosbestic point emerges at 485 nm for decay times longer than 1.6 ps. The remaining GSB (λ > 400 nm) does not follow the inverted steady-state absorption (SSA, Fig. S21(A)), indicating that the ESA extends to shorter wavelengths until approx. 420 nm. Note that the decay of the long wavelength ESA reduces also the GSB in the first 8 ps.

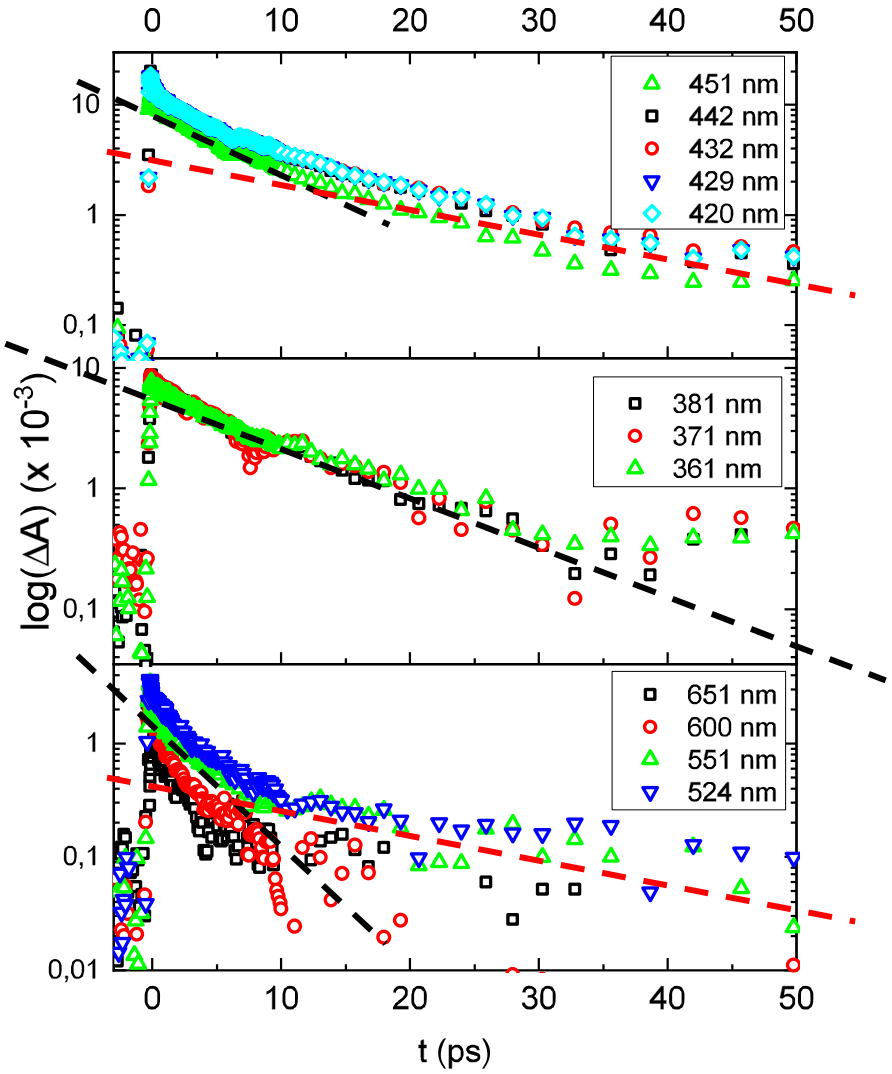

Figure S22: Relevant kinetics traces in the different zones of C2: main band of GSB in the top, minor band of GSB in the center and ESA in the bottom. Dashed lines are guide-to-the-eye for an evaluation of the multi-component character of the decay. Their slopes represent τ_2 and τ_3.

In Fig. S22 the kinetic traces are reported in semi-log scale. In the top the ones related to the main band of GSB, between 420 and 451 nm, are displayed. We plot here log(-GSB(t)). three-component. All of them show a decay in the same range of times. Only the kinetic trace at 451 nm is slightly faster than the others that are perfectly overlapped. By visual inspection, we identify a first decay time on a sub-picosecond time scale, followed by a slower 3-5ps decay (black dashed line, decay by a factor of

10, in 10-12 ps) and a third component in the 15-20 ps range (red dashed line). In the central panel the traces related to the minor band of GSB (<400 nm) are reported. These show an almost mono-exponential decay due to the smaller S/N ratio. The 15-20 ps component emerges barely above the noise floor (≈ 2-3 10^{-4}, at neg. delay times) at longer delays. We have to note that in all the kinetics traces of the GSB (both bands) a 3-5 ps decay is present. The kinetics of the ESA are reported in the bottom panel of Fig S21. At long wavelengths (651-600 nm), the decay is dominated by a sub-3 ps time scale, but when bluer traces are investigated (551-554 nm) the longer 15-20 ps lifetime comes out of the noise floor.

The single kinetic traces are fitted by the equation (1)

$$F(t) = \left[\sum_{i=1}^{n} a_i e^{-t/\tau_i}\right] \otimes IRF \qquad (1)$$

Where *n* is the number of the kinetic species, a_i is the amplitude associated to the decay time τ_i. Following the above visual inspection n=3 is used for all wavelengths. The sum is convoluted with the Instrument Response Function (IRF) that is assumed to have a Gaussian shape, centered at t=0 with 70 fs FWHM.

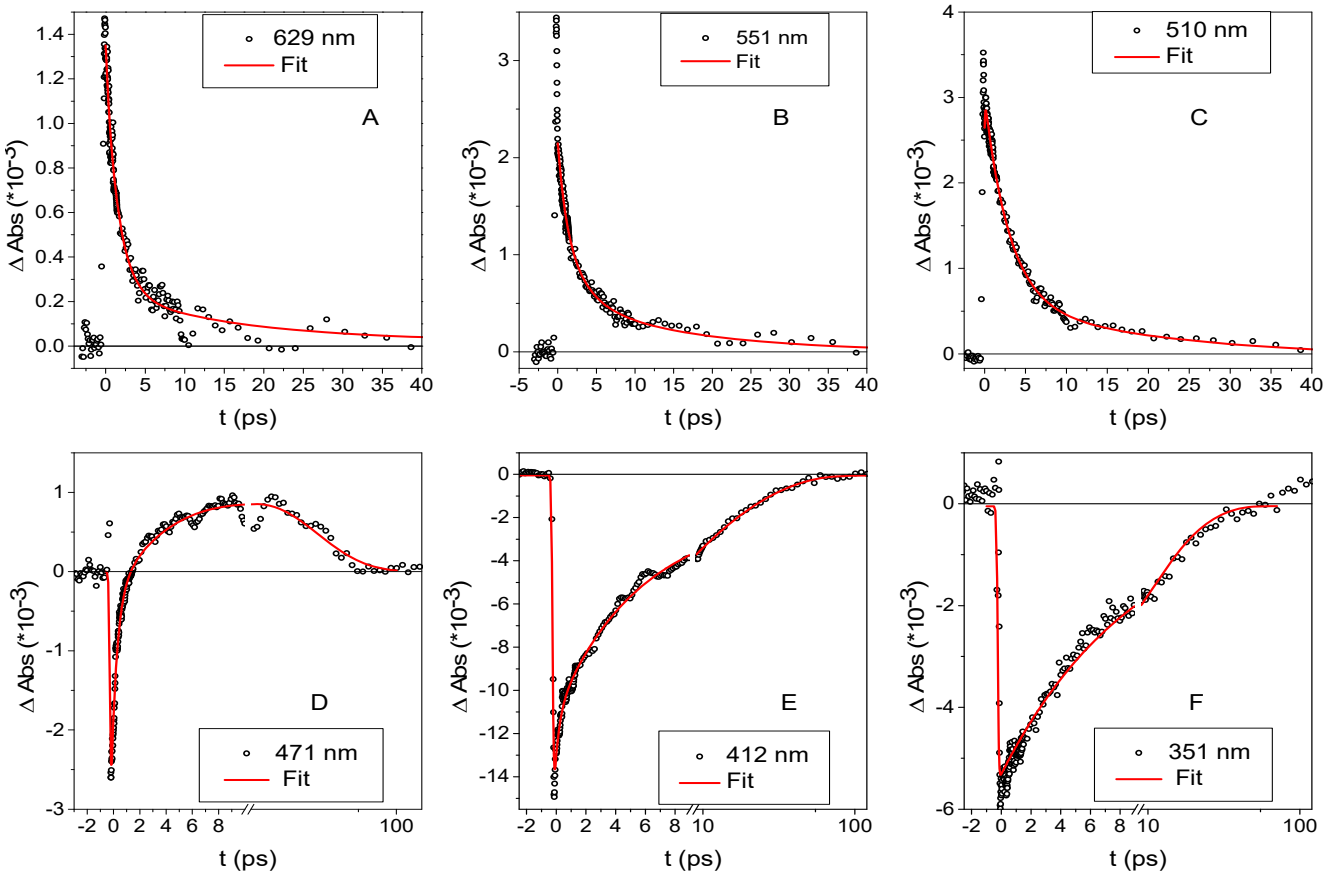

Figure S23: Examples of kinetic traces of **C2** and their fits. Note the linear scaling of the time axis for t≤10 ps and logarithmic thereafter. Panels A to C : ESA ; (D) : Crossover from bleach to ESA ; (E) and (F) : GSB. The contributions of the three lifetimes are apparent : τ_1 in the first picosecond, τ_2 up to 10 ps and the slow τ_3

Some single kinetics and the relative fit of **C2** are displayed in Fig S23; the parameters are reported in Table S3. The strong wavelength dependency of the fitted decay times cuts short on a global fitting approach.

Table S3 Fit parameters obtained by single kinetic analysis of C2 in AcN. the three decay times in ps and their corresponding amplitudes. "*" denote fixed values not optimized by the fit procedure (too low amplitude). The error bars are in the 10-20% range for τ_1 and τ_2. Values for τ_2 and τ_3 are rounded accordingly.

Wl (nm)	τ (ps)	τ2 (ps)	τ3 (ps)	A_1	A_2	A_3
351	0.30	9.4	18*	0.00	-5.70E-03	2.92E-04
364	0.30	4.7	19	2.22E-04	-4.79E-03	-2.83E-03
381	0.04	4.5	17	0.00*	-5.26E-03	-2.76E-03
412	0.30	4.1	16	-4.27E-03	-6.13E-03	-5.34E-03
429	0.33	4.7	18	-6.49E-03	-7.73E-03	-4.81E-03
451	0.33	3.3	13	-3.73E-03	-5.34E-03	-4.93E-03
451	0.39	4.0	16*	-3.64E-03	-6.24E-03	-3.79E-03
461	0.35	5.4	20*	-3.90E-03	-5.68E-03	5.00E-04
470	0.42	5.6	20	-2.95E-03	-2.43E-03	2.05E-03
480	0.40	2.9	22	-2.10E-03	5.30E-04	2.12E-03
490	0.58	2.6	19	-1.52E-03	2.20E-03	1.88E-03
500	0.22	3.0	18	-1.71E-03	2.49E-03	1.20E-03
510	0.06	3.0	21	-7.27E-03	2.58E-03	6.81E-04
520	0.05	2.7	21	-6.96E-03	2.40E-03	5.20E-04
535	0.05	2.2	20	-4.60E-03	2.01E-03	5.93E-04
551	0.40	2.0	16*	3.53E-04	1.57E-03	6.17E-04
580	0.40	2.1	18*	6.43E-04	1.34E-03	2.83E-04
605	0.63	3.5	16*	8.38E-04	8.38E-04	9.59E-05
630	0.40	1.7	16*	2.17E-04	1.14E-03	2.30E-04
647	0.50	1.9	16*	2.25E-04	1.42E-04	1.42E-04

In Fig. S22 the decay times vs wavelength and the amplitudes vs wavelength are reported. At longer wavelengths (>550 nm) the ESA band is dominated by the A_1 and A_2 while A_3 is negligible. τ_1 has an

average value of 0.4 ps. It appears both in the ESA and GSB decay and is related to fast vibrational cooling and/or intersystem crossing from the ^{1}MLCT state. As such it appears as a rise time for the ESA in the 500-540 nm range. τ_2 and τ_3 are almost independent of wavelength with average values of 4±1 ps and 18±3 ps, respectively. In the red part of the spectrum τ_2 is decreasing, indicating spectral narrowing of the ESA spectrum due to vibrational cooling. In table S2 all the parameters are reported; '*' indicates an imposed fixed time needed for a meaningful fit of the kinetics. The value is taken in average with the neighboring wavelengths. The amplitude associated with τ_3 is in agreement with the 15 ps spectrum of Fig. S17 (top panel). In the range 440-600 nm has a positive amplitude while below it is always negative (GSB). The amplitude of τ_2 is in agreement with the evolution described in Figs. S19 and B. Indeed, the spectral shape of A_2 is consistent with the long wavelength ESA component revealed after subtraction of the 15 ps spectrum (fig. S21(B)). Most importantly, A_2 has a significant amplitude (30-40% larger than A_3) in the GSB region.

If we associate τ_2 and τ_3 with different excited states X and Y and their populations, the spectral shape of A_2 allows us to discriminate between a parallel and a sequential excited state relaxation scheme (fig. 7 in main paper). In the sequential scheme, the population moves from X to Y without any ground state bleach recovery. The 4 ps component should thus appear as a rise time (neg. A_2) for the ESA of Y in the 450-500 nm range. This is partly true since A_2 is negative for λ< 470 nm, but not for the wavelengths of maximum ESA of state B (470-490nm). Hence, a clear indication of X giving rise to Y is lacking. More importantly is the observation of the GSB recovery occurring dominantly with τ_2, for λ< 470 nm. This is in contradiction to the sequential relaxation scheme, but fully in agreement with the parallel one. Indeed, both the decay of the population of X and Y lead to ground state recovery.

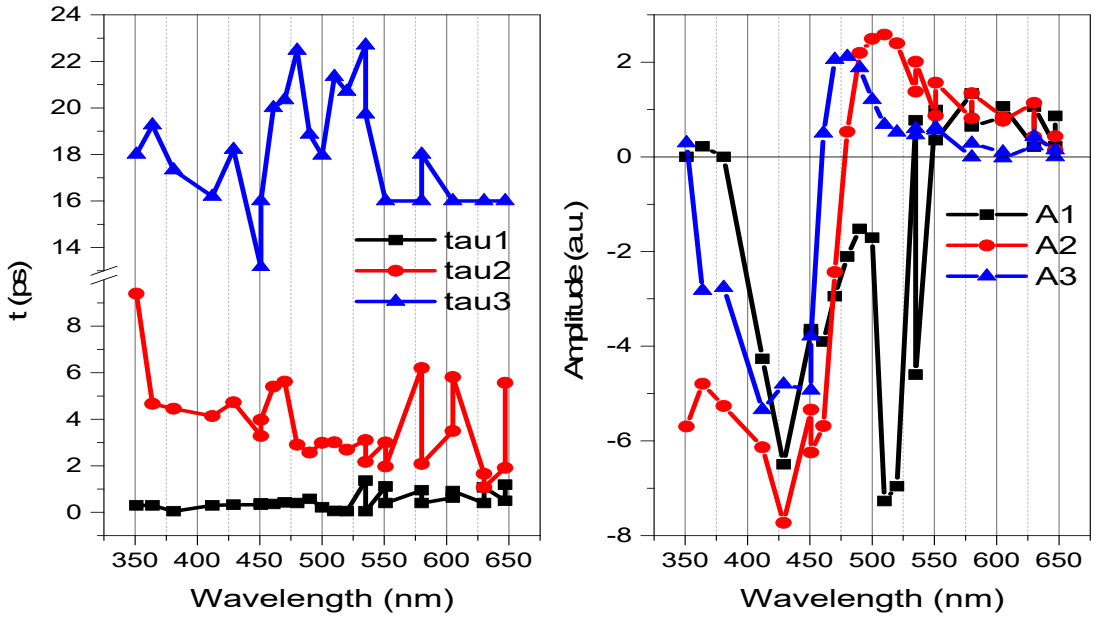

Figure S24. Time vs wavelength on the left and amplitude vs wavelength on the right. Plot of the table S1.

Analysis of spectra and kinetic traces of C1

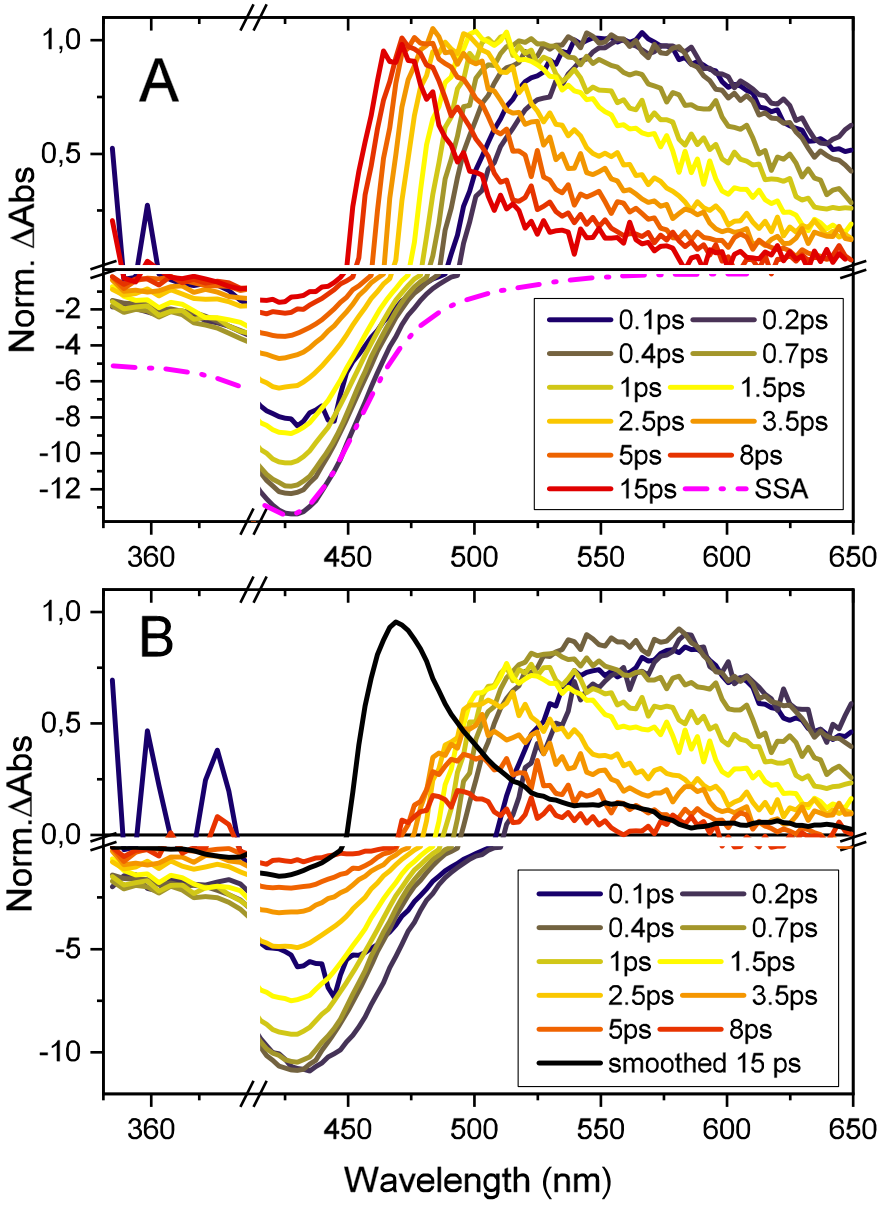

Figure S25: Selected spectra of **C1** in AcN at different times normalized on the maximum of ESA band (A). The inverted steady-state absorption spectrum is shown for comparison (dash-dotted line). Spectra minus the smoothed spectrum at 15 ps in the bottom (B).

The same analysis is performed for **C1**-fac/mer-mixture. In Fig. S25A the early time spectra are normalized on the maximum of the ESA band. As for the previous sample, the evolution of the positive band is highlighted (narrowing and shift), as is the difference in the GSB with respect to the inverted SSA (dashed line). After the normalization, a continuous evolution is still observed in all the signals. Only the spectra at 15 and 35 ps are overlapping. As discussed in the main text, the minor band of the GSB (<400 nm) has not the same intensity as the reversed SSA, normalized on the other negative band, due to a hidden ESA. Differently to **C2**, this band has a time decay that follows the main one. Panel B shows the same normalized spectra, but after subtraction of the normalized and smoothed 15 ps spectrum. This isolates the ESA contribution at longer wavelengths, which, unlike for **C2**, displays a continuous shift over 40 nm within the first 8 ps (Fig S25-B). The continuous shift goes along with the absence of an isosbestic point until 5 ps. Only the spectrum at 8 ps has an intersection with the 5 ps

one at 470nm. As for **C2**, the three bands are not equivalently affected by the 15 ps spectrum subtraction.

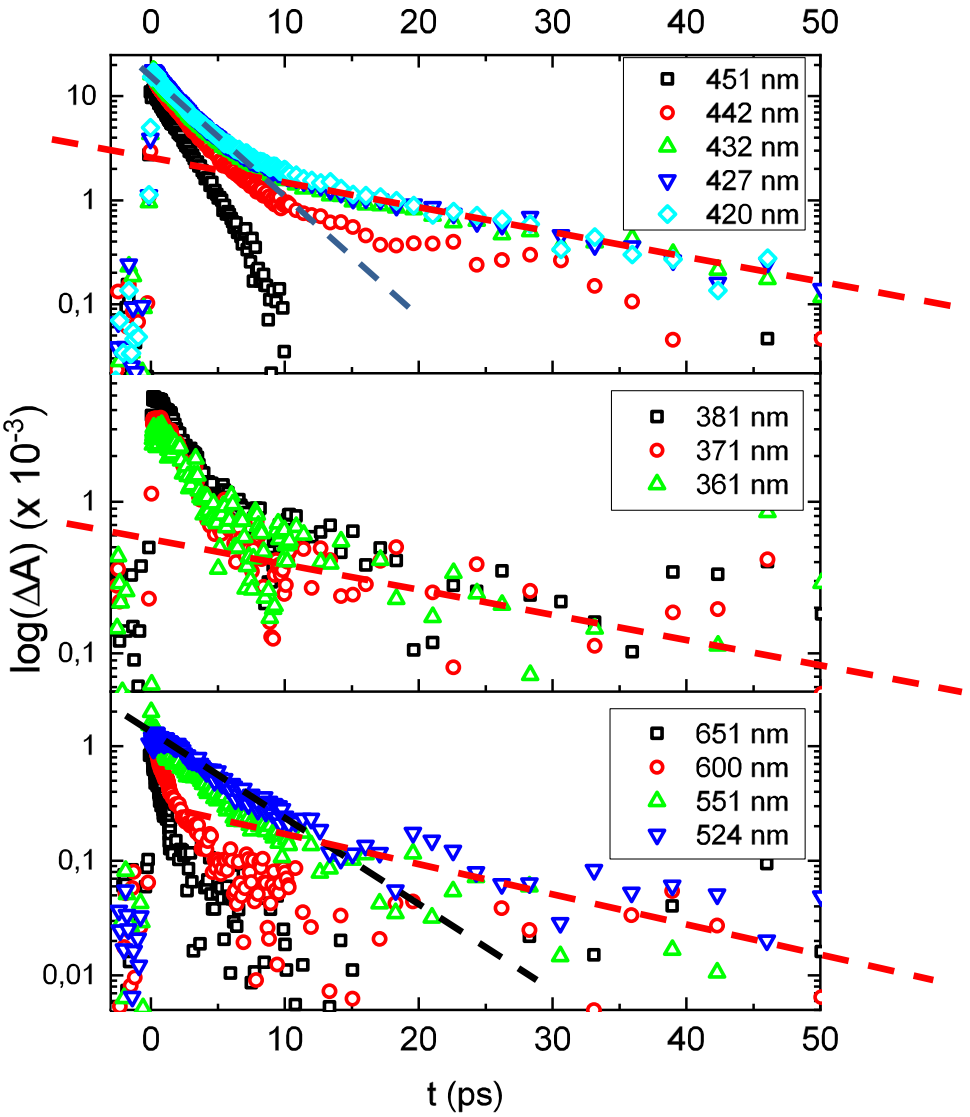

Figure S26: Relevant kinetics traces in the different spectral zones of **C1**: main band of GSB in the top, minor band of GSB in the center and ESA in the bottom.

In Fig. S26 some relevant kinetic traces are reported in semi-logarithmic scale. In the top panel the inverse of the main band of GSB is shown (log(-GSB)). The wavelength dependency is very clear on these signals, indeed the kinetics related to the central part of the band (420-432 nm) completely overlap. Note that unlike C2, the GSB is reduced to 5% of the t=0 value within 10 ps. It is apparent from the different slopes that the kinetic traces decay on two times scales, i.e. 2-3 and 18-20 ps. A zoom into the first picosecond reveals an additional sub-picosecond decay (not shown). The 442 nm trace has the same trend, but the timescale is slightly faster. The 451 nm trace is mono-exponential, as this wavelength corresponds to the ESA/GSB crossover of the longer-lived component (cf. Fig. S25). This kinetic trace allows therefore to determinate very accurately τ_2. In the central panel the kinetics related to the minor band of the GSB are reported. All of them have the same trend (completely overlapped). Interestingly, they are almost constant during the first picosecond. The amplitude of the slower τ_3 component is almost in the noise floor.

As for **C2**, the ESA has different kinetics according to the wavelength observed. i.e. for wavelength longer than 600 nm the decay is ultrafast (decay to 10% within <3 ps), while for shorter ones the long 15-ps component is coming out of the noise level.

To understand if the signal comes from both isomers or from only one, a second example of **C1** with a different isomer ratio (87.5% of Mer isomer, in the mixture 1:8, compared to 92.8 % , in the 1:14 mixture) is tested. In Fig. S27, the kinetic traces at 427 nm are reported in semi-logarithmic scale. Within the noise level of the measurement, the two curves are perfectly overlaying so we can conclude that the signal is largely dominated by the **C1**-mer while the *fac* isomer can be considered as an impurity.

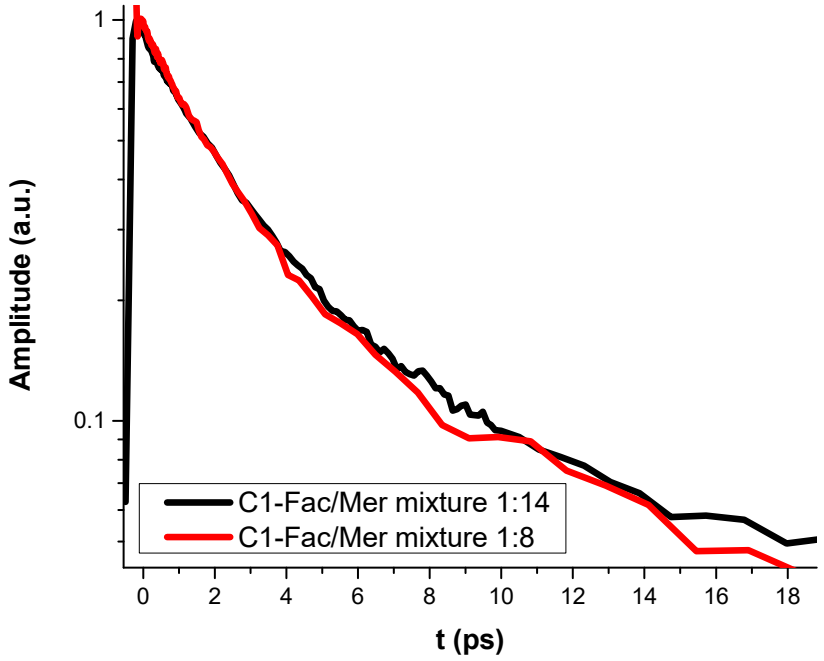

Figure S27 Inverse GSB kinetic trace at 427 nm of C1 mixture at different isomer ratios excited at 400nm.

According to the visual inspection (Fig. S27), the kinetics traces of the 1:14 C1 are fitted by Eq 1, by a 3-exponential fit and obtained fit parameters are reported in table S2. Some kinetics and the related fits are displayed in Fig. S28. The traces are fitted by three decay components, even when only two or one are necessary but in these cases the amplitude is zero (if $\leq 10^{-5}$). According to this, some values must be fixed and they are characterized by *.

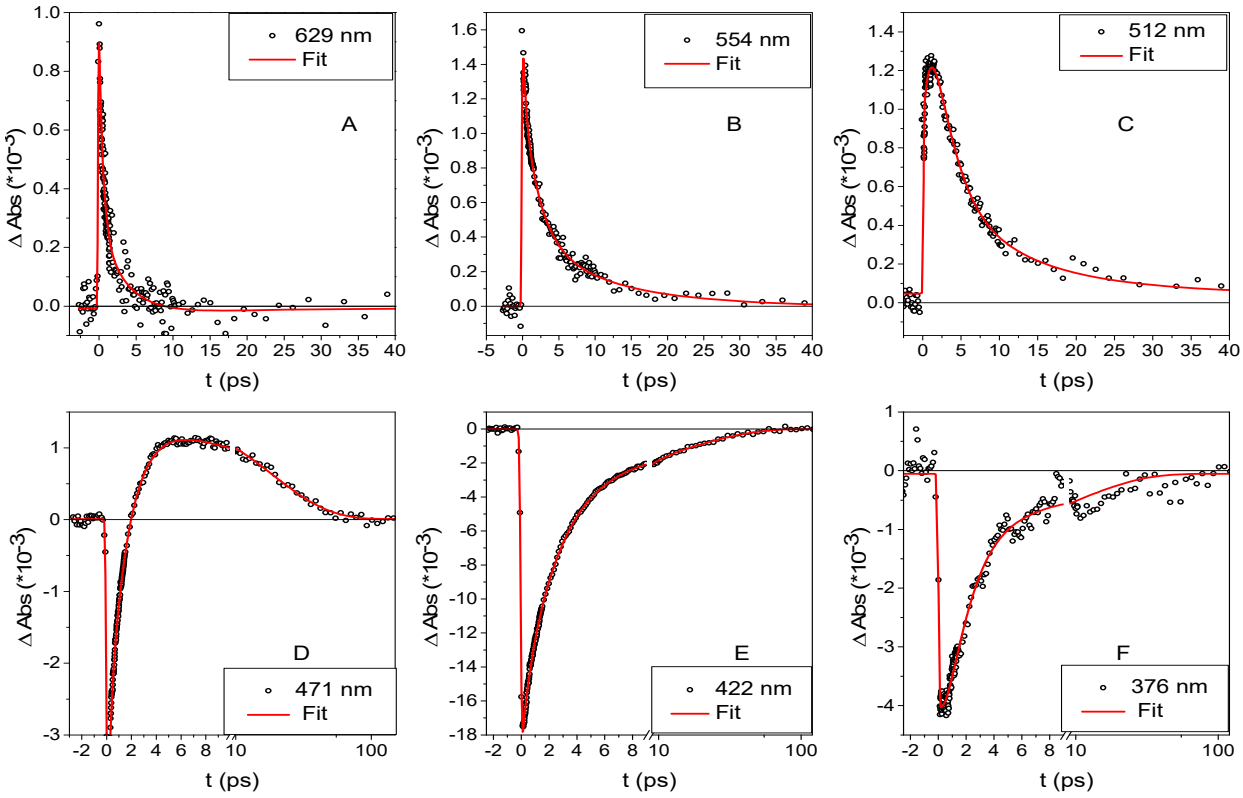

Figure S28: Examples of kinetic traces and their fits od C1. Note the linear scaling of the time axis for t≤10 ps and logarithmic thereafter. Panels A to C : ESA ; (D) : Crossover from bleach to ESA ; (E) and (F) : GSB. The contributions of the three lifetimes are apparent: τ_1 in the first picosecond, τ_2 up to 10 ps and the slow τ_3 decay thereafter.

In Fig. S29, the results of table S4 are plotted. In the right panel, the time vs wavelength is reported while the amplitude vs wavelength is on the left. τ_1 is, in average, 0.5 ± 0.3 ps, τ_2 is 2.5 ±0.7 ps and τ_3 is in the range of 18 ps. More interesting is the right graph when the amplitudes are plotted as a function of wavelength. The ESA band (λ >550 nm) is dominated by τ_2 and τ_1 while the amplitude of τ_3 is zero. In the range 500-550 nm, only the short component has a negative amplitude while the others are positive. We assign τ_1 to rapid electronic/vibrational relaxation in the excited state contributing as a rise time for both ESA bands (450-550 nm). As we discussed before (Fig S19 A) the ESA bands overlap with the GSB, leading to imperfect agreement of the latter with the reverse SSA, in particular in the 450-500 nm range when a_3 is positive. Remarkably, in the GSB region 475-350 nm the main contribution is due to τ_2 that generates the GSB signal. Unlike for **C2**, τ_3 contributes only to 20% (at 425 nm) to the GSB. Its amplitude is nevertheless larger than the percentage of fac isomers in this mixture, confirming our hypothesis that both decay processes are borne by the mer isomer only. More importantly, both τ_2 and τ_3 are associated with the GSB recovery. In conclusion, the same parallel relaxation scenario holds for the fac/mer mixture as for the fac-only complexes. The main difference between the two samples is in the larger amplitude of τ_2, and a value of 2.5 ±0.7 ps for the mer isomers, instead of 4.0±1.0 ps for fac, leading to an overall faster excited state decay.

Table S4: Results of the single wavelength fits of **C1** in AcN: the three decay times in ps and their corresponding amplitudes. "*" denote fixed values not optimized by the fit procedure (too low amplitude). The error bars are in the 10-20% range for lifetimes τ_1 and τ_2. Values for τ_2 and τ_3 are rounded.

λ (nm)	τ1 (ps)	τ2 (ps)	τ3 (ps)	A_1	A_2	A_3
651	0.55	3.6	17*	8.24E-04	3.42E-04	-4.39E-05
600	0.34	2.0	17*	8.22E-04	8.56E-04	-7.54E-06
571	0.23	2.0	17*	8.60E-04	9.15E-04	2.59E-04
541	0.01	2.6	17*	0.00*	9.31E-04	4.36E-04
532	0.55	3.2	17*	-3.00E-04	1.05 E-3	4.30E-04
522	0.59	4.0	17*	-8.65E-04	1.45 E-3	1.89E-04
512	0.99	2.8	17*	-1.6E-3	1.33 E-3	8.91E-04
502	1.10	2.9	17*	-1.54 E-3	1.48 E-3	7.88E-04
493	1.22	3.4	18	-1.95 E-3	1.51 E-3	8.48E-04
481	0.80	3.0	15	-2.3 E-3	-1.60 E-3	1.78 E-3
471	0.29	1.7	18	-1.48 E-3	-5.09 E-3	1.74 E-3
461	0.42	2.1	20	-2.07 E-3	-7.84 E-3	1.26 E-3
451	0.68	2.5	18	-3.21 E-3	-10.67 E-3	3.09E-04
442	0.22	2.3	17	-3.57 E-3	-13.88 E-3	-1.33 E-3
432	0.36	2.5	18	-2.95 E-3	-14.88 E-3	-2.29 E-3
422	0.34	2.5	17	-2.33 E-3	-14.66 E-3	-2.83 E-3
376	0.82	1.5	17*	4.63 E-3	-7.49 E-3	-1.09 E-3
364	0.58	1.7	17*	2.51 E-3	-4.25 E-3	-7.20E-04
356	0.35	1.9	17*	6.10 E-3	-3.59 E-3	-8.90E-04

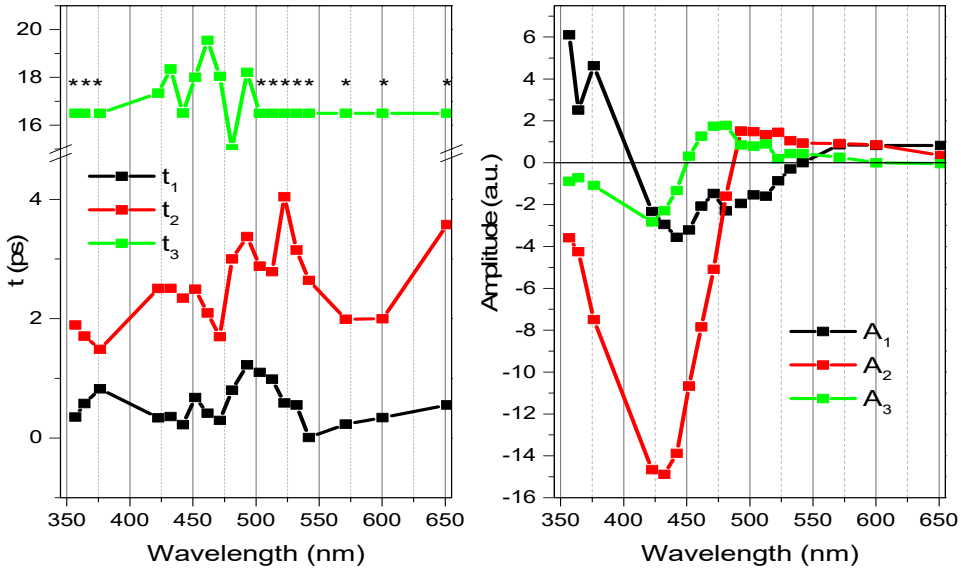

Figure S29: Time vs wavelength on the left and amplitude vs wavelength on the right. Plot of the table S5.